Design, synthesis and 3D-QSAR studies of novel 1,4-dihydropyridines as TGFβ/Smad inhibitors

11 AUTHORS, INCLUDING:

Brigita Vigante
Latvian Institute of Organic Synthesis
72 PUBLICATIONS **163** CITATIONS

SEE PROFILE

Gunars Duburs
Latvian Institute of Organic Synthesis
463 PUBLICATIONS **1,445** CITATIONS

SEE PROFILE

Carsten Strohmann
Technische Universität Dortmund
307 PUBLICATIONS **3,501** CITATIONS

SEE PROFILE

Dennis Schade
Technische Universität Dortmund
30 PUBLICATIONS **269** CITATIONS

SEE PROFILE

Original article

Design, synthesis and 3D-QSAR studies of novel 1,4-dihydropyridines as TGFβ/Smad inhibitors

Daniel Längle [a], Viktoria Marquardt [a], Elena Heider [a], Brigita Vigante [b], Gunars Duburs [b], Iveta Luntena [b], Dirk Flötgen [a], Christopher Golz [a], Carsten Strohmann [a], Oliver Koch [a], Dennis Schade [a, *]

[a] TU Dortmund University, Department of Chemistry & Chemical Biology, Otto-Hahn-Str. 6, 44227 Dortmund, Germany
[b] Latvian Institute of Organic Synthesis, Aizkraukles 21, Riga LV-1006, Latvia

ABSTRACT

Targeting TGFβ/Smad signaling is an attractive strategy for several therapeutic applications given its role as a key player in many pathologies, including cancer, autoimmune diseases and fibrosis. The class of b-annelated 1,4-dihydropyridines (DHPs) represents promising novel pharmacological tools as they interfere with this pathway in a novel fashion, i.e. through induction of TGFβ receptor type II degradation. In the present work, >40 rationally designed, novel DHPs were synthesized and evaluated for TGFβ inhibition, substantially expanding the current understanding of the SAR profile. Key findings include that the 2-position tolerates a wide variety of polar functionalities, suggesting that this region could possibly be solvent-exposed within the (thus far) unknown cellular target. A structural explanation for pathway selectivity is provided based on a diverse series of 4″-substituted DHPs, including molecular electrostatic potential (MEP) calculations. Moreover, the absolute configuration for the chiral 4-position was determined by X-ray crystal analysis and revealed that the bioactive (+)-enantiomers are (R)-configured. Another key objective was to establish a 3D-QSAR model which turned out to be robust ($r^2 = 0.93$) with a good predictive power ($r^2_{pred} = 0.69$). This data further reinforces the hypothesis that this type of DHPs exerts its novel TGFβ inhibitory mode of action through binding a distinct target and that unspecific activities that would derive from intrinsic properties of the ligands (e.g., lipophilicity) play a negligible role. Therefore, the present study provides a solid basis for further ligand-based design of additional analogs or DHP scaffold-derived compounds for hit-to-lead optimization, required for more comprehensive pharmacological studies in vivo.

© 2015 Elsevier Masson SAS. All rights reserved.

1. Introduction

The superfamily of transforming growth factor-β (TGFβ) ligands comprises of a series of structurally closely related cytokines that modulate a plethora of cellular processes such as cell division, proliferation, differentiation, migration, adhesion and apoptosis in a tissue context-specific manner [1]. They play a key role during embryogenesis but also for homeostasis in adult tissues. Disruption or pathologic alterations of these pathways are associated with a number of diseases such as cancer, autoimmune diseases and fibrosis [2]. Therefore, the pharmacologic modulation of TGFβ-dependent processes is of great therapeutic relevance, underlined by the many 'biologicals' and small molecules currently in clinical trials for distinct applications [3,4]. In general, three strategies are being investigated for therapeutic intervention with TGFβ signaling: 1) inhibition at the translational level by anti-sense oligonucleotides, 2) blockade of ligand—receptor interaction using antibodies and 3) inhibition of TGFβ receptor kinases (TGFβRI + II) by small molecules [4,5]. The latter approach provides several advantages over biological agents, because small molecules can be administered orally and may reach and infiltrate target tissues more efficiently than biomacromolecules. In addition, target and pathway selectivity can often be greater by using defined and pharmacologically optimized small molecule agents [6]. In this regard, the herein presented compound class of dihydropyridines might be of particular therapeutic value in a regenerative medicine setting.

We previously reported on a novel class of TGFβ inhibitors, *b*-annelated 1,4-dihydropyridines (DHPs), which were identified in a phenotypic screen for small molecules that stimulate cardiac differentiation of stem cells, with ITD-1 (**1**) as the hit compound (Fig. 1) [7]. It was shown that these DHPs inhibit TGFβ signaling via a novel mode of action, which is the downregulation of the TGFβ type II receptor (TGFβRII), giving these 1,4-DHPs the name ITDs (*i.e.*, inducers of TGFβ receptor degradation). This novel mechanism sets these compounds apart from the "classic" TGFβ inhibitors that typically target the receptor kinase domains, with the consequence of redundant activity on closely related signaling pathways or kinases, respectively. An initial focused medicinal chemistry study was done which revealed a rather steep SAR profile for the observed biological activity [8].

Here, we report on the extension of these SARs with additional, more versatile substituted and functionalized derivatives addressing distinct shortcomings of our current SAR picture of these compounds (Fig. 1). Along these lines, it was key to determine the — up to now — unknown absolute configuration of the active (+)-enantiomers. In addition, the entire dataset known until today was used to establish a quantitative correlation between structure and activity via a 3D-QSAR analysis. The primary aim was here to further reinforce the selective nature of observed TGFβ inhibiting activity, possibly addressing one relevant target and ruling out unspecific effects in the cellular assays. This work eventually sets the basis for the design of novel DHPs or DHP scaffold-derived compounds for rational hit-to-lead optimization that will allow conducting more comprehensive pharmacological studies in an *in vivo* setting.

2. Results and discussion

2.1. Chemistry

As indicated in the introduction, our preliminary understanding of the structure activity relationships for this novel class of TGFβ/Smad signaling inhibitors has been limited and generated rather lipophilic derivatives which, accordingly, suffer from the respective pharmaceutical and pharmacokinetic shortcomings (*e.g.*, solubility, ADME aspects, formulation technologies). Therefore, several DHP derivatives were designed to incorporate heteroatom-containing, polar functional groups but also to explore steric aspects of certain regions of the molecules.

Scheme 1 summarizes the synthetic routes to novel DHPs with various substituents in 2-, 3-, 4-, 6- and 7-position. Using such classic Hantzsch conditions, it was possible to access many of the desired compounds **1**, **6**–**21** with yields ranging from 17 to 68%. Through replacement of the β-dicarbonyl component **2** (mostly dimedone) with appropriate acetylenedicarboxylates **3**, 2,3-diester substituted DHPs were readily available. Notably, these 2-carboxylic ester groups could be selectively hydrolyzed under basic conditions (*i.e.*, 3 equiv of NaOH in EtOH) to give the free carboxylic acids **20a** and **21a** in good yields (68–87%) without compromising the 3-esters. This underlines the more stable carbamate nature of the 3-esters through conjugation with the 1,4-DHP core. For the introduction of a nitrogen atom in position 6 (X = NH, Scheme 1), piperidine-2,4-dione instead of dimedone (**2**) was used and gave compound **12** in 36% yield.

If the desired aldehyde was not commercially available, 4′-bromophenyl-derivative **7** was prepared as the starting material and subsequently coupled under Suzuki conditions to afford compounds **22**–**32** in yields between 15 and 77% under non-optimized conditions (Scheme 2). For compound **32** the *O*-TBDMS-protected 4-hydroxyphenylboronic acid was used in the Suzuki reaction, followed by deprotection with TBAF in THF.

Moreover, two polycyclic 1,4-dihydropyridines were synthesized according to the general Hantzsch concept, *i.e.* decahydroacridine **34** and hexahydroindeno[1,2-*b*]quinoline **36** (Scheme 3). For these compounds, however, it was necessary to first isolate the initial condensation products under distinct cyclization conditions.

2-Amino-substituted 1,4-dihydropyridines were accessible by refluxing amidinoacetic acid ethyl ester **38**, dimedone **37** and aldehyde **39** in a sodium ethanolic solution as described in the literature (Scheme 4) [9].

However, in order to access more basic amines in 2-position (*i.e.*, not conjugated with the DHP core, vinylogous carbamate), the use of a terminal amino group in the alkane-1,3-dione derivative for the Hantzsch DHP synthesis proved challenging. For this reason, the 2-bromomethyl compound **42** was prepared in moderate yields (51%) according to a procedure described by Petrova et al., treating ITD-1 (**1**) with NBS for 3 days (Scheme 5) [10]. In fact, this 2-bromomethyl intermediate proved to be a key intermediate to install several functional groups in 2-position. **42** was then reacted with potassium phthalimide as a protected precursor of the primary amino derivative. Unfortunately, after removing the protecting group, the desired free amine could not be isolated due to cyclization to lactame **43**. Although a primary amine was not accessible via the routes described above, secondary amines **44** and **45** could be successfully prepared and isolated as hydrochlorides in 27% and 58% yields after reacting 2-bromomethyl intermediate **42** with ethylamine or *n*-propyl amine, respectively.

Furthermore, the above described condensation reaction causing cyclization to a 5-membered ring (*i.e.*, pyrrolo[3,4-*b*]quinolone) was used to explore a series of different tricyclic derivatives (Scheme 5). Aside from this *N*-unsubstituted secondary lactam **43**, the corresponding benzyl- and ethyl-analogs were prepared. *N*-ethyl lactam **46** was accessible from the *N*-ethylaminomethyl-substituted DHP **44** in good yields (59%) under basic conditions. An attractive alternative to this reaction was discovered when

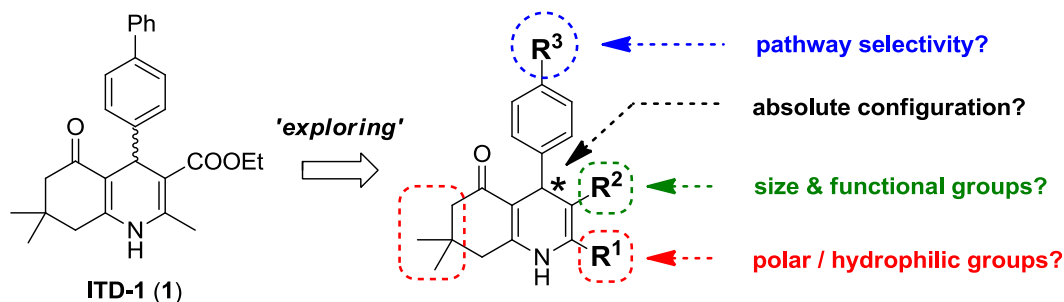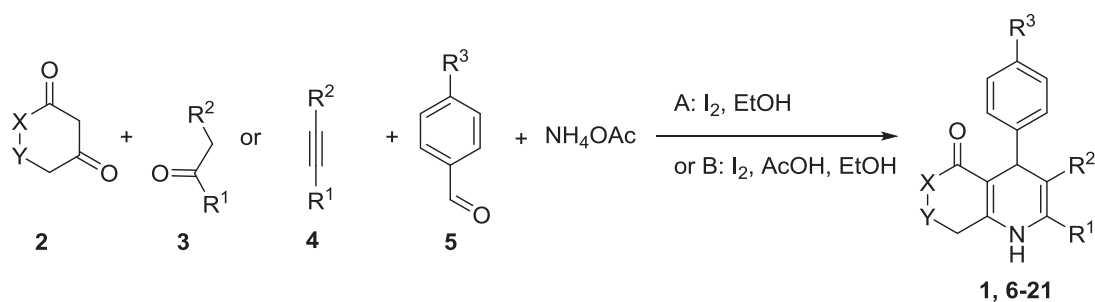**Fig. 1.** Chemical structure of cardiogenic *b*-annelated 1,4-DHPs as TGFβ/Smad inhibitors, with ITD-1 (**1**) as the "hit compound" from preliminary studies [8], highlighting regions of the molecule to be explored for expanding key SAR features.

cmpd	X	Y	R^1	R^2	R^3	yield	route
1	CH$_2$	CMe$_2$	Me	COOEt	Ph	38%	A
6	CH$_2$	CMe$_2$	Me	COOEt	Br	40%	A
7	CH$_2$	CMe$_2$	Me	COOEt	4–BrPh	38%	A
8	CH$_2$	CMe$_2$	Me	COOEt	Ethinyl	37%	A
9	CH$_2$	CMe$_2$	Me	CONHEt	Ph	17%	A
10	CH$_2$	CMe$_2$	Me	COOtBu	Ph	33%	A
11	CH$_2$	CMe$_2$	Me	COOAllyl	Ph	23%	A
12	NH	CH$_2$	Me	COOEt	Ph	36%	A
13	CH$_2$	CMe$_2$	Me	COOC$_{12}$H$_{25}$	Ph	71%	B
14	CH$_2$	CMe$_2$	Me	COnPr	Ph	55%	B
15	CH$_2$	CMe$_2$	Me	COnBu	Ph	21%	B
16	CH$_2$	CMe$_2$	Et	COEt	Ph	31%	B
17	CH$_2$	CMe$_2$	Me	CONHBn	Ph	68%	B
18	CH$_2$	CMe$_2$	Me	COO(CH$_2$)$_2$OnPr	Ph	67%	B
19*	CH$_2$	CMe$_2$	Me	CN	Ph	33%	B
20	CH$_2$	CMe$_2$	COOMe	COOMe	Ph	42%	B
21	CH$_2$	CMe$_2$	COOEt	COOEt	Ph	53%	B

Scheme 1. Synthetic routes to novel TGFβ inhibiting *b*-anellated 1,4-DHPs with various substituents in 2-, 3-, 4-, 6- and 7-position. * β-Aminocrotononitrile instead of alkane-1,3-dione component and NH$_4$OAc was used.

incorporating the desired amine in the form of the 2-carboxylic amide **17** (see Scheme 1) [8] followed by treatment with NBS for 24 h, furnishing the desired *N*-benzylated pyrrolo[3,4-*b*]quinolone **55** in 81% yield (not shown in any Scheme, see Experimental section). In a similar approach, reacting 2-bromomethyl intermediate **42** with KOH (in chloroform) did not provide access to the primary alcohol since this intermediate rapidly cyclized to furo[3,4-*b*]qui-nolone **47**. Still, a non-cyclized analog (*i.e.*, 2-methoxymethyl DHP,

48) was successfully obtained in high yields (91%) after treating **42** with KOH in methanol.

For the preparation of 1,4-dihydropyridines carrying distinct ester groups in 3-position, and which were not accessible by the general procedure outlined in Scheme 1, a protocol was used that proved useful for similar derivatives in the past (Scheme 4) [8]. The already above described possibility for orthogonal deprotection of the 2-carboxylic esters under basic conditions, while leaving the 3-
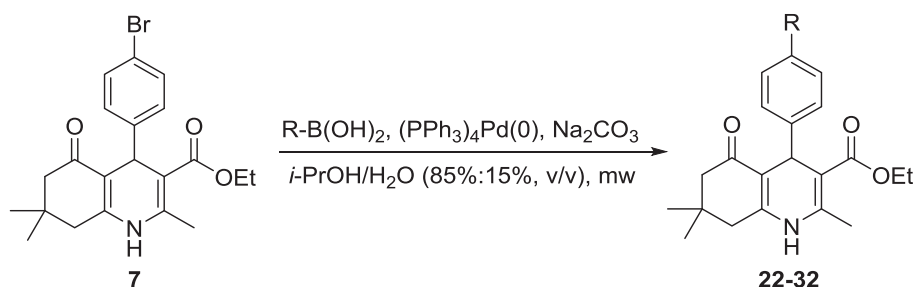
cmpd	R	yield
22	4''-CF$_3$-Ph	77%
23	4''-SO$_2$Me-Ph	77%
24	4''-Cl-Ph	76%
25	4''-F-Ph	72%
26	4''-OCF$_3$-Ph	52%
27	4''-CN-Ph	50%
28	4''-Pyridinyl	46%
29	4''-CH$_3$-Ph	39%
30	4''-NMe$_2$-Ph	36%
31	4''-OMe-Ph	25%
32	4''-OH-Ph	15% (2 Steps)

Scheme 2. Synthesis of novel 4′-substituted *b*-annelated 1,4-DHPs.

esters intact, implies a high chemical stability of the latter. In fact, hydrolysis of ethyl ester **1** to carboxylic acid **49** could only be accomplished under strongly Lewis acidic conditions with BCl$_3$. Subsequent alkylation with different alkyl bromides and potassium carbonate in DMF delivered the desired esters **50**–**53**.

2.2. X-ray crystal structure analysis

In our earlier reports, we elaborated on the fact that the observed activity on cardiomyocyte differentiation from murine embryonic stem cells and inhibition of TGFβ signaling is linked to the (+)-enantiomers [7,8]. Interestingly, these mechanistic studies also revealed that the stereoselective mode of action was reversed for calcium channel antagonism since only the (−)-enantiomers strongly inhibited calcium transients in rat cardiomyocytes whereas the TGFβ inhibiting (+)-enantiomers were weakly active [8].

One of the designated goals of our ongoing work is to define a detailed picture of the *b*-annelated DHPs' pharmacophore for novel ligand-based approaches, especially since the cellular target has not yet been identified. A key requirement was thus to determine the absolute configuration of the active (+)-enantiomer of ITD-1 (**54b**) by X-ray crystallography. For this, the synthesis of single enantiomers was done as reported before, *i.e.* via diastereomeric threonine-based 3-esters [8]. However, it was crucial to use

enantiomers of highest possible optical purity for crystallization. High enantiomeric purity was achieved after separating diastereomeric intermediates by preparative HPLC (eluent: H$_2$O/ACN/MeOH, 30/27/43) instead of the previously reported tedious procedure that used gravity flow chromatography with a toluene/EtOAc eluent system. Using this method, the ITD-1 (+)-enantiomer **54b** was prepared in 23% yields over three steps and an optical purity of >98%*ee* $\left(a\frac{20}{D} = +74 \right)$ (lit. +68) [8], and could be crystallized for X-ray analysis by slow evaporation of an ethanolic solution.

The crystal structure of **54b** revealed that the cardiomyogenic, TGFβ inhibiting (+)-enantiomer is (*R*)-configured as depicted in Fig. 2a. In accordance with recently reported x-ray crystal data on differently 4-substituted, *b*-annelated DHPs [11], the typical structural features of classic 1,4-dihydropyridines are conserved for these DHPs, such as the flattened boat conformation and the pseudoaxial orientation of the 4-substituent. Notably, however, the dihedral (torsion) angle of 107° for the C4–C5–C18–C19 plane relative to the C6–C7 plane is rather shallow (**54b**), compared to similar DHPs, *e.g.* a ring-open (non-fused) 4-biphenyl analog (91–92°, torsion angle) [11] or a *b*-annelated 4-phenyl analog (97–99°, torsion angle) [12]. This becomes also obvious comparing
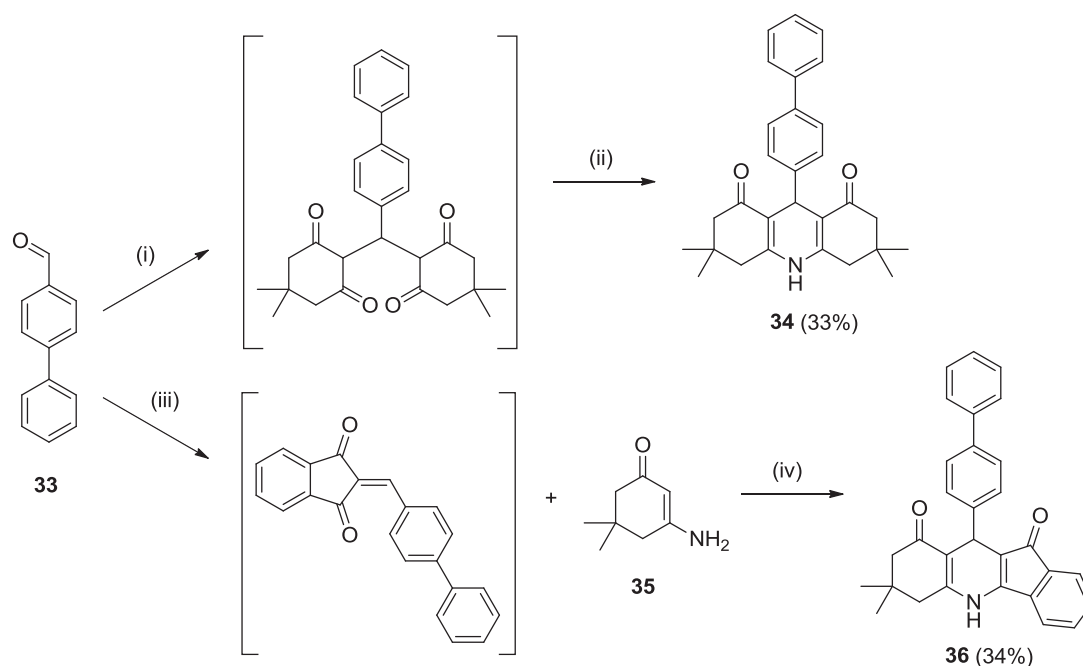
Scheme 3. Synthetic routes to novel polycyclic 1,4-DHPs. Reagents and conditions: (i) Dimedone, piperidine, EtOH, H$_2$O; (ii) NH$_4$OAc, AcOH, 33% (2 steps); (iii) Indane-1,3-dione, AcOH, H$_2$SO$_4$; (iv) AcOH, 34% (2 steps).

R = Ph (**40**, 12%)
R = *t*Bu (**41,** 20%)
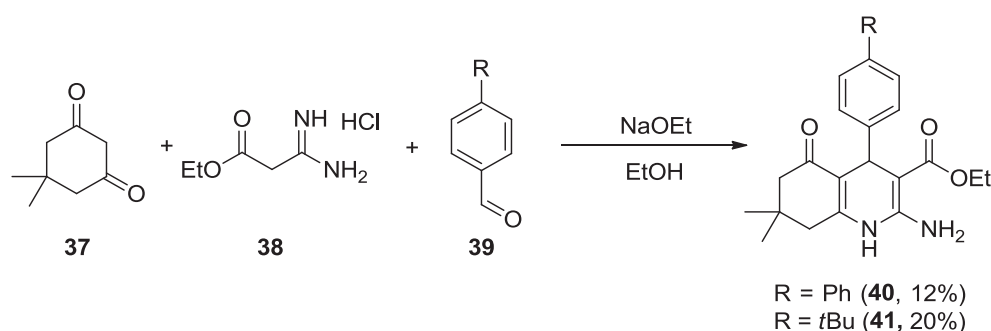
Scheme 4. Synthesis of novel 2-amino-substituted *b*-annelated 1,4-DHPs.

the angles of 4-biphenyl substituents above the DHP core, with 118.9° for **54b** and 104.3° and 116.3° for the ring-open 4-biphenyl analog or annelated 4-phenyl analog, respectively (see Supporting information, Figs. S1–S3). To which extent these conformational aspects play a role in the context of TGFβ inhibition remains to be clarified and is subject of our current research.

2.3. TGFβ/Smad inhibition

As outlined in the Introduction, we aimed at expanding on our preliminary SAR info for this subclass of *b*-annelated 1,4-DHPs as cardiomyogenic TGFβ inhibitors. This SAR has been steep and generated rather lipophilic derivatives aside from the fact the many regions of the molecule were not explored at all. Therefore, the newly synthesized compounds were designed to incorporate heteroatom-containing, polar functional groups but also to explore steric aspects of certain regions of the molecules. Compounds were evaluated in a TGFβ/Smad reporter gene assay in HEK293T as described before [8], and the data is summarized in Table 1.

Thus far, the 2-position of these DHPs as TGFβ inhibitors has not been investigated at all. We tested several carboxylate, ether and amino functionalities for activity and found that quite a few groups are indeed well-tolerated. For example, replacing the lipophilic 2-methyl group by a 2-amino group decreased potency only to a low extent. 2-Amino DHP **40** had an IC$_{50}$ value of 1.3 μM compared to 0.8 μM of its methyl analog ITD-1 (**1**). The respective 4′-*t*-Bu analog **41** was ranging even in the submicromolar range (*i.e.*, IC$_{50}$ = 0.5 μM) implicating that the introduction of a 2-amino group still provides access to the most potent DHP-based TGFβ inhibitors.

Since the direct attachment of an amino group to the DHP core does not generate a 'true amine' but a vinylogous carbamate instead, we reasoned to keep a methylene group spacer and introduced the ethyl (**44**, IC$_{50}$ = 3.4 μM) and *n*-propyl (**45**, IC$_{50}$ = 1.6 μM) amines. Both of the amines revealed loss in potency which was moderate compared to the 2-amino analog **40** (IC$_{50}$ = 1.3 μM) but at least 2-fold when compared to the parent DHP **1** (IC$_{50}$ = 0.8 μM). However, this little loss in potency may well be compensated when decorating other regions of the molecule with known affinity-increasing substituents, while at the same time buying-in an improved aqueous solubility.

Interestingly, several *O*-functionalized analogs were also still active. 2-Methyl ether derivative **48** showed a TGFβ inhibitory activity of 78% at 2.5 μM (IC$_{50}$ = 1.8 μM). Even replacement of the 2-methyl group with carboxylic esters rendered the molecules active, although losing potency by ca. 2-fold (**20** and **21**, IC$_{50}$'s = 2.0 and 1.8 μM) compared to DHP-1. As exemplified with two derivatives
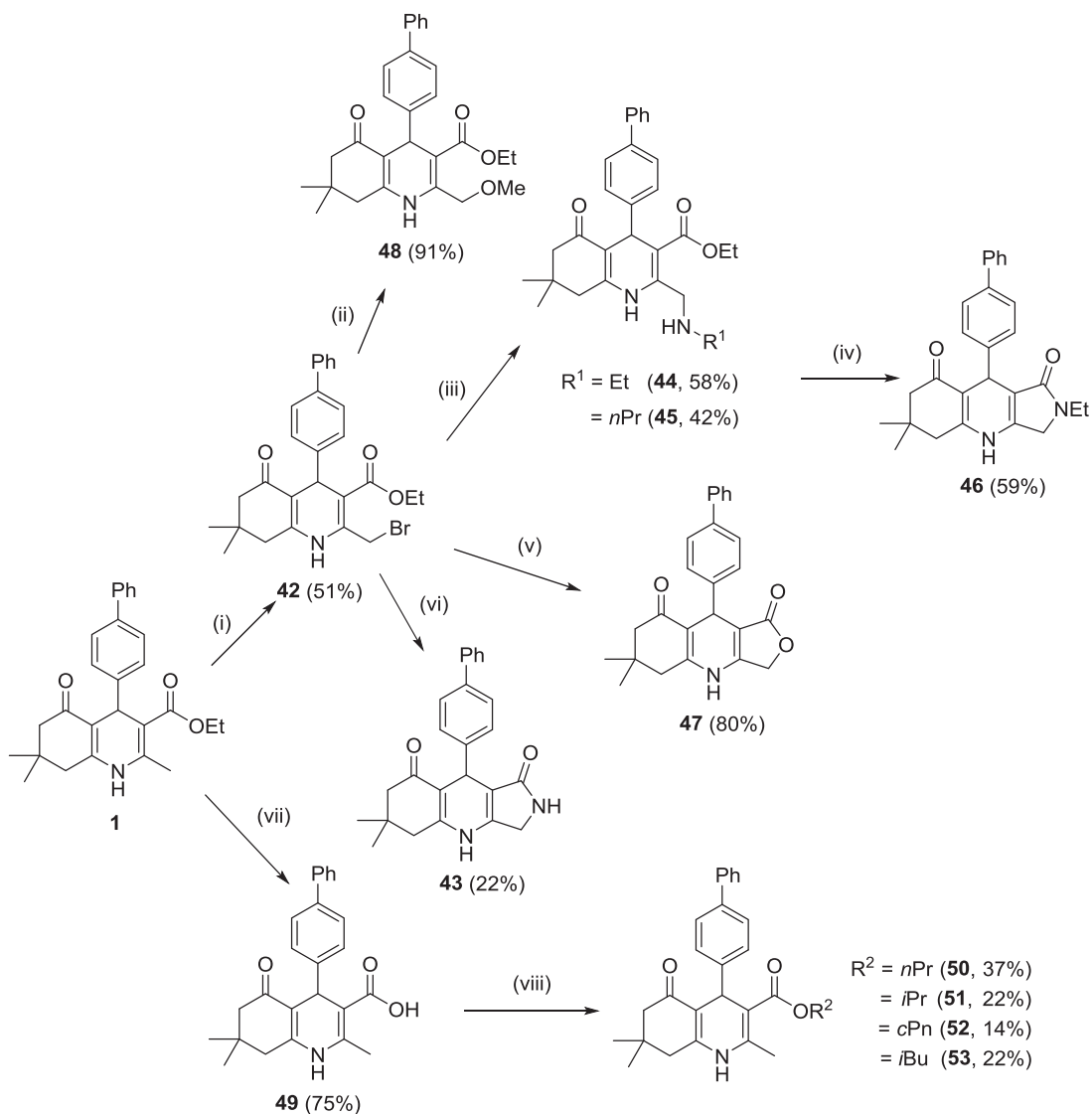
Scheme 5. Synthetic routes to novel 2- and 3-substituted *b*-annelated DHPs. Reagents and conditions: i): NBS, MeOH; ii): KOH, MeOH; iii): H$_2$NR^1, DCM; iv): KOH, EtOH; v): KOH, CHCl$_3$; vi): Potassium phthalimide, DMF; H$_2$NCH$_3$, 22% (2 Steps); vii): BCl$_3$, DCM; viii): R^{2}Br, DMF.

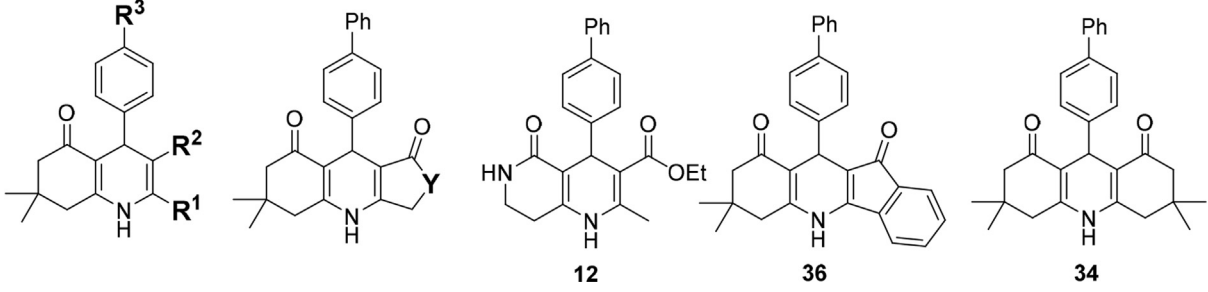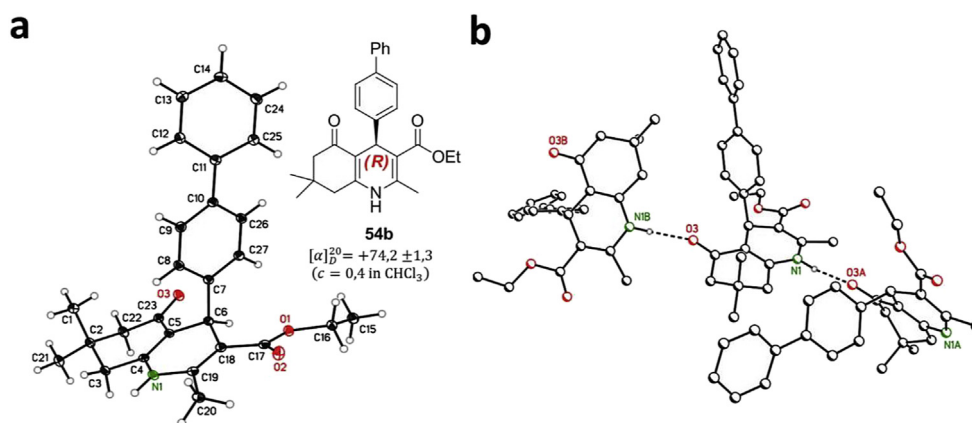**Fig. 2.** X-ray crystal structure analysis of the cardiomyogenic, TGFβ inhibiting (*R*)-configured ITD-1 (+)-enantiomer **54b**. a) ORTEP plot, chemical structure and optical rotation data; b) Packing diagram of the title compound showing intermolecular hydrogen bonds between N1 and the carbonyl oxygen of the *b*-annelant (symmetry codes: A = 2 − y, 1 + x − y, 1/3 + z; B = 1−x + y, 2 − x, −1/3 + z).

Table 1
TGFβ inhibition of novel *b*-annelated 1,4-dihydropyridines.[a]

Compd	R^1	R^2	R^3	Y	IC_{50} (μM)	%Inhibition (2.5 μM)
1	Me	COOEt	Ph	–	0.85 ± 0.30	83 ± 8
40	NH_2	COOEt	Ph	–	1.33 ± 0.21	61 ± 2
41	NH_2	COOEt	*t*Bu	–	0.51 ± 0.03	89 ± 5
44	CH_2NHEt	COOEt	Ph	–	3.44 ± 0.33	64 ± 27
45	CH_2NHnPr	COOEt	Ph	–	1.60 ± 0.38	57 ± 6
48	CH_2OMe	COOEt	Ph	–	1.89 ± 0.33	78 ± 14
20	COOMe	COOMe	Ph	–	2.01 ± 0.60	46 ± 16
20a	COOH	COOMe	Ph	–	n.d.	4 ± 5
21	COOEt	COOEt	Ph	–	1.80 ± 0.20	56 ± 6
21a	COOH	COOEt	Ph	–	n.d.	0 ± 2
50	Me	COO*n*Pr	Ph	–	0.49 ± 0.24	93 ± 3
51	Me	COO*i*Pr	Ph	–	0.66 ± 0.13	85 ± 3
11	Me	COOAllyl	Ph	–	0.62 ± 0.02	91 ± 5
10	Me	COO*t*Bu	Ph	–	0.67 ± 0.17	84 ± 1
53	Me	COO*i*Bu	Ph	–	0.42 ± 0.27	91 ± 3
52	Me	COO*c*Pn	Ph	–	1.11 ± 0.52	77 ± 12
18	Me	$COO(CH_2)_2OnPr$	Ph	–	n.d.	0 ± 3
13	Me	$COOC_{12}H_{25}$	Ph	–	n.d.	0 ± 18
9	Me	CONHEt	Ph	–	n.d.	31 ± 1
17	Me	CONHBn	Ph	–	5.19 ± 3.45	32 ± 13
19	Me	CN	Ph	–	2.95 ± 0.68	44 ± 6
16	Et	COEt	Ph	–	1.63 ± 0.56	62 ± 8
14	Me	CO*n*Pr	Ph	–	0.50 ± 0.13	84 ± 11
15	Me	CO*n*Bu	Ph	–	0.56 ± 0.11	80 ± 2
22	Me	COOEt	4″-CF_3Ph	–	0.97 ± 0.29	88 ± 6
29	Me	COOEt	4″-CH_3Ph	–	0.35 ± 0.03	94 ± 2
26	Me	COOEt	4″-OCF_3Ph	–	0.48 ± 0.06	95 ± 1
32	Me	COOEt	4″-OHPh	–	0.73 ± 0.26	74 ± 6
31	Me	COOEt	4″-OCH_3Ph	–	0.42 ± 0.21	93 ± 4
24	Me	COOEt	4″-ClPh	–	0.76 ± 0.22	91 ± 2
7	Me	COOEt	4″-BrPh	–	0.46 ± 0.25	94 ± 3
25	Me	COOEt	4″-FPh	–	1.23 ± 0.02	74 ± 16
30	Me	COOEt	4″-NMe_2Ph	–	0.33 ± 0.15	95 ± 2
23	Me	COOEt	4″-SO_2MePh	–	2.76 ± 0.18	44 ± 1
27	Me	COOEt	4″-CNPh	–	1.79 ± 0.42	52 ± 2
28	Me	COOEt	4″-Pyridinyl	–	6.14 ± 1.55	27 ± 11
8	Me	COOEt	Ethinyl	–	1.71 ± 0.60	59 ± 5
47	–	–	–	O	4.30 ± 1.71	37 ± 4
43	–	–	–	NH	n.d.	28 ± 8
46	–	–	–	NEt	5.03 ± 1.31	25 ± 15
55	–	–	–	NBn	0.87 ± 0.20	82 ± 5
12	–	–	–	–	n.d.	21 ± 2
36	–	–	–	–	1.26 ± 0.01	70 ± 2
34	–	–	–	–	1.88 ± 0.27	55 ± 6

n.d., not determined.
[a] Data represent means ± SD of n = 2–4 independent experiments in a TGFβ/Smad reporter gene assay.

(**20a** and **21a**), a carboxylic acid group pointed out the limitation of introducing a negatively charged moiety in the 2-position since both compounds were inactive. However, it cannot be excluded that this phenomenon is solely due to the limited cell permeability of such free acids. Taken together, these findings support the hypothesis that the region surrounding the 2-position could possibly be solvent-exposed, and is rather not key for high-affinity interaction with its unknown cellular target.

Next, further building on the 3-carboxylic acid (ester) group, several strategic SAR extensions were realized. Starting off with esters of specific size and branching we could support the

hypothesis that particularly C_3–C_4 containing esters were most potent (*i.e.*, IC_{50} = 0.5–0.7 μM), while groups larger than C_4 were detrimental to biological activity. Similar hints were already obtained in our previous study [8]. To address the question whether a simple increase in lipophilicity and/or enrichment in lipid membranes could contribute to potent TGFβ inhibition in a cellular assay setup, long chain ethylene glycol (**18**) and fatty (lauryl) alcohol (**13**) linker moieties were evaluated but turned out inactive.

Importantly, the electronic and H-bond donor/acceptor qualities of the direct 3-substituent were evaluated. Switching from the ethyl ester **1** to the respective amide **9** (inactive) revealed that an H-
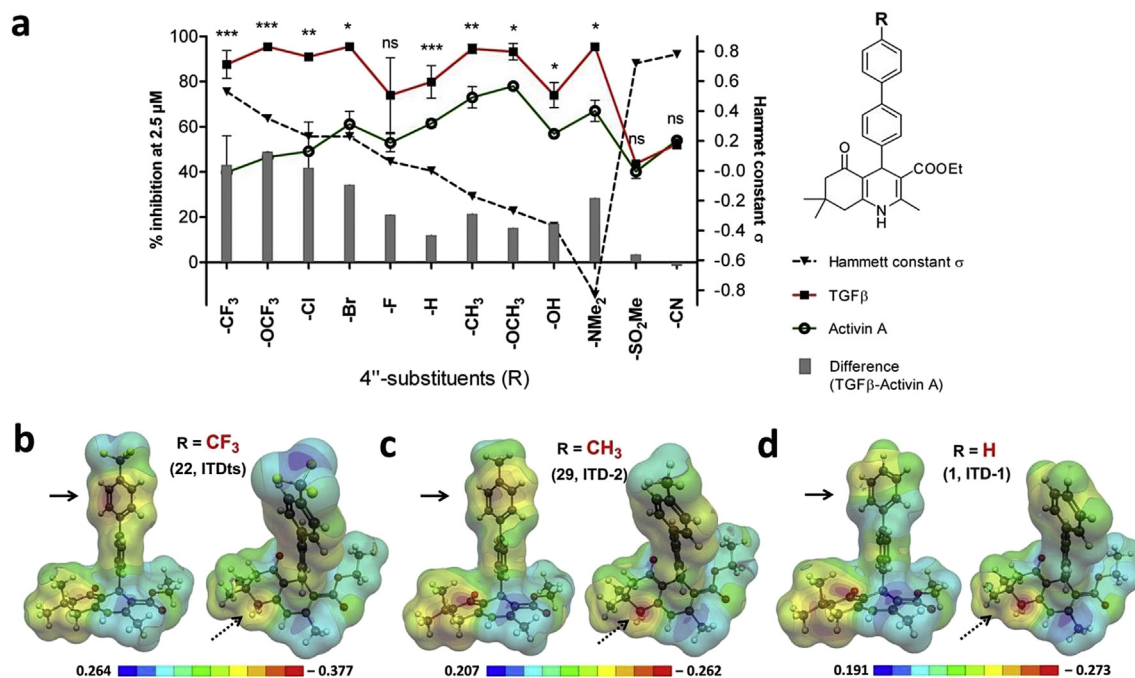
Fig. 3. Structural basis for pathway selective inhibition of *b*-annelated DHPs: a) TGFβ versus Activin A. Inhibition values were determined in a Smad4-binding element (SBE4) reporter gene assay in HEK293T cells using either TGFβ-2 or Activin A for pathway induction [8]. Data represent means ± SD ($n = 2$–4), normalized to DMSO controls (=0% inhibition). Statistical analysis: Two-paired student t-test p values: *** ($p \leq 0.0001$), ** ($p \leq 0.001$), * ($p \leq 0.05$), ns (not significant). b and c) Connolly surface (probe radius = 1 Å) mapped with the molecular electrostatic potential (MEP), quantum chemical calculations performed with Gaussian 03 (revision E.01); Blue/red areas represent negative/positive electrostatic potentials. (For interpretation of the references to colour in this figure legend, the reader is referred to the web version of this article.)

bond donor diminishes TGFβ inhibitory activity. This finding is in accordance with the fact that the free 3-carboxylic acid is also inactive [8]. An interesting observation was the moderate but still surprisingly high potency of a simple 3-cyano derivative (**19**, $IC_{50} = 2.9$ μM), considering that a clear SAR and increase in potency was typically obtained for proper-sized alkyl residues which were completely lacking here. This raised the question of the significance of the H-bond acceptor properties close to the DHP core. Therefore, a series of ketones (**14**–**16**) were introduced that indeed further underlined the relevance of this H-bond acceptor. Based on the 3-substituent chain length, the direct ketone analog to ITD-1 (**1**, $IC_{50} = 0.8$ μM) turned out to have high TGFβ inhibitory potency (**14**, $IC_{50} = 0.5$ μM).

Together, we have now compelling evidence that a specific and important molecular interaction originates from the 3-position. In particular H-bond acceptor properties, exemplified with a simple ketone, together with a C_3–C_4 aliphatic, low-branched side chain defines the spatial and electronic requirements for this TGFβ inhibitor pharmacophore. In a similar approach, via incorporation of a nitrogen at the 6-position, *i.e.* the *b*-annelation site of the DHPs, the same question was addressed as to whether an amide (lactam) abolished activity (**12**, 20% inhibition at 2.5 μM).

From our previous endeavors with this compound class, the significance of the 4-substituent was evident and has been further explored ever since. Although this region of the molecule does not permit modifications that would alter the linear orientation along the 4-phenyl-4′ axis, a distinct 4″-substitution pattern of the biphenyl turned out to be key for the desired signaling pathway selectivity, *i.e.* TGFβ versus Activin A [8]. In fact, a 4″-CF₃-substituted DHP **22** did exert a higher inhibitory efficiency against TGFβ versus Activin A compared to its 4″-CH₃ analog **29**. In order to provide a more comprehensive, SAR-based explanation to verify this inhibitory profile, a larger series of 4″-substituted DHPs were designed, synthesized and tested against both of these TGFβ

superfamily ligands. The assay data results are summarized in Table 1 (TGFβ inhibition) and further illustrated in Fig. 3 (TGFβ versus Activin A inhibition), which reveals a clear SAR trend based on the Hammett constant of the 4″-substituents. Although overall inhibitory potency against TGFβ was comparably high for compounds bearing either electron-withdrawing (=**7**, **22**, **24**, **25**, **26**) or -donating groups (=**29**, **31**, **32**, **30**) of certain size (74–95% inhibition at 2.5 μM), this activity did not parallel the determined anti-Activin A activity. For the latter, the electronic nature of this 4″-substituent indeed made a difference: DHPs containing electron-withdrawing groups consistently exhibited a low interference with Activin A signaling, *e.g.* <50% inhibition for **22** (4″-CF₃), **26** (4″-OCF₃) and **24** (4″-Cl). In accordance with this data, it was tempting to speculate that a further increase of pathway selectivity could be realized through incorporation of 4″-substituents with even higher Hammett constant values than the OCF₃ or CF₃ groups. Therefore, sulfone DHP **23** and nitrile **27** were synthesized and tested. However, the outcome was disappointing since not only pathway selectivity was completely abrogated but also overall inhibitory potency was significantly diminished. Concluding from these results, a small-sized electron withdrawing 4″-substituent, devoid of π-bonds, ensures the highest degree of selectivity against TGFβ over Activin A inhibition.

In an attempt to explain the distinct pathway inhibitory profiles of 4″-electron-withdrawing and -donating group substituted DHPs, molecular electrostatic potentials (MEPs, Fig. 3b–d) were calculated for **22** (4″-CF₃), **29** (4″-CH₃) and the 4″-unsubstituted ITD-1 (**1**). Interestingly, against our intuitive expectation that electron-withdrawing substituents in 4″-position would generate an electron-deficient distal aromatic ring, the connolly surface of **22** (Fig. 3b) revealed the opposite: The 4″-CF₃ group creates an electron-rich distal aromatic by pulling electron density from the proximal 4-phenyl into the distal ring (solid arrow, Fig. 3b).

This finding supports the idea that this distal region of the

molecule is important for potent (selective) interaction with the unknown cellular target and possibly several of the examined 4''-substituents exert additional beneficial effects due to specific molecular interactions within the pocket of the unknown target. Obviously, the effect is less pronounced for a 4''-CH$_3$-substituted (**29**, Fig. 3c) or 4''-unsubstituted DHP (**1**, Fig. 3d). Therefore, illustration of MEP connolly surfaces did not only extend the Hammett constant-based explanation of pathway selectivity (Fig. 3a), it also provided an unexpected insight into electron density distribution of this series of 4-biphenyl DHPs. In this regard, yet another surprising observation was a high electron density above the C8-methylene group in the *b*-annelant (dashed arrows, Fig. 3b–d) which was expected to be rather around the N1 atom of the DHP core. The generation of an electron-rich center above the *b*-annelant may represent one explanation for the fact that annelation is required for TGFβ inhibiting activity.

In addition to a simple SAR extension of the 2-, 3- and 4-substituents, it was vital for our understanding of the pharmacophore to increase the chemical space of these DHPs. A series of compounds was synthesized and tested which contained an additional 5-membered *d*-annelant. Lactams **43** and **46** as well as lactone **47** were weakly active underlining that the increase in rigidity negatively affects the desired activity. An exception was the *N*-benzyl derivative **55** that was comparably potent to the original ITD-1 with an IC$_{50}$ of 0.8 μM, and therefore, represents an 'outlier' of the thus far devised SAR model for which we do not have an explanation yet. However, this finding prompted us to explore other, even larger tri- and tetracyclic structures. With the indenone **36** an aromatic residue was incorporated in analogy to the active *N*-benzyl lactam **55**, but obviously much less floppy. Interestingly, **36** was also still quite active (IC$_{50}$ = 1.26 μM), similar to the symmetric tricyclic aliphatic derivative **34** (IC$_{50}$ = 1.88 μM).

2.4. 3D-QSAR studies

Quantitative structure activity relationships (QSAR) describe the correlation of biological activity with the chemical structure of a set of molecules. QSAR analyses have become a widely used technique in drug design [13] since their first description in 1964 by Hansch and Free-Wilson [14,15]. They are commonly used to validate structure activity relationships as well as to predict the biological activity of newly designed compounds. This approach is intrinsically most powerful when building on data from biochemical assays with compound activities covering a broad dose–response range. Nevertheless, also for cell-based data, 3D-QSAR information can be of high value. In fact, such *in vitro* cellular studies have been applied for the validation and QSAR analysis of biological activities of several 1,4-dihydropyridine-type of compounds, for example regarding antitumor activity in HL-60 cells [16], inhibition of amyloid beta peptide accumulation in CHO cells [17], antitubercular activity in a BACTEC 460 assay system [18], aside from classic calcium channel antagonist activity in guinea pig ileum smooth muscle assays [19]. In all cases, the requirement for calculating a QSAR model is the assumption that all evaluated derivatives share the same target or target binding site, and unspecific effects, such as permeability, have no significance influence or do not decisively determine the desired activity, respectively.

In the context of the TGFβ inhibitors described herein, the cellular target has not yet been identified. Thus, the aim was in the first place to support the hypothesis that these type of *b*-annelated 1,4-DHPs exert their novel TGFβ inhibitory mode of action through binding a distinct target in case the observed SAR can be quantitatively captured. Unspecific activities that would derive from intrinsic properties of the ligands (*e.g.*, lipophilicity) rather than from direct interaction with the target binding site were supposed
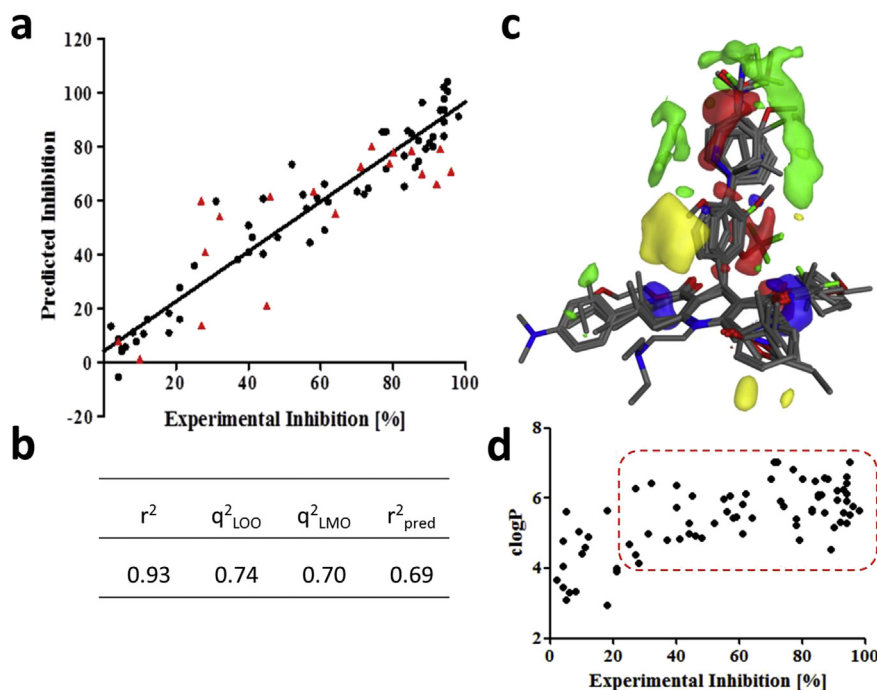

Fig. 4. 3D-QSAR analysis results of TGFβ inhibitory activities of DHPs. a) Predicted versus experimental inhibition of the trainings dataset (black circles, black line) and of the test dataset (red triangles). b) Statistical parameters of the final 3D-QSAR model. c) Alignment of trainings data set and Van-der-Waals and electrostatic contour maps for 3D-QSAR model (green/yellow: steric bulky regions are positively/negatively correlated with inhibitory activity; red/blue: positively/negatively charged substituents are positively correlated with inhibitory activity). d) Correlation plot of calculated logP (clogP) versus TGFβ inhibition (% at 2.5 μM). (For interpretation of the references to colour in this figure legend, the reader is referred to the web version of this article.)

to be ruled out. At the same time, of course, unspecific ligand features or "off-target" effects always play a role in cell- and organism-based assay systems.

A 3D-QSAR analysis was performed using TGFβ inhibitors from this study and our previous report that showed a "measurable activity" which led to a training dataset of 58 DHPs and a final test dataset of 19 DHPs. The 3D conformations of all ligands were prepared based on the crystal structure of the active, (R)-configured ITD-1 (+)-enantiomer **54b** that we disclosed here for the first time. Since the absolute configuration at the 4-position is vital for the compounds' TGFβ inhibitory activity, this information was likewise important for a reliable 3D-QSAR model.

Although dealing with cell-based data from a reporter gene assay, the model had a high r^2 of 0.93 and significant, good values for the internal cross-validation ($q^2_{LOO} = 0.74$, $q^2_{LMO} = 0.70$), which indicates a robust model (Fig. 4b). However, the predictive power of this model on a test dataset (*i.e.*, that was not involved in the training dataset) is the most challenging and most important part of a QSAR analysis. The final test dataset (19 compounds) revealed an r^2_{pred} of 0.69 which confirmed the predictive power of the obtained 3D-QSAR model. Overall, a significant and robust model with predictive power could be devised for the DHP dataset which supports the assumption that a defined target (binding site) or mechanism is addressed.

One advantage of 3D-QSAR modeling is the visualization of molecular interaction field coefficients as contour maps. The alignment of the 58 compound-comprising training data set is shown in combination with the contour map of the model in Fig. 4c. Yellow contours highlight regions where steric bulky substituents correlate negatively with inhibitory activity and whereas bulky substituents within the green ones correlate positively. Moreover, electrostatic interactions that correlate positively with the biological activity are shown in red (negative partial charges) and blue (positive partial charges). Of course, the detailed influence of substituents on electrostatic potential as shown in Fig. 3b–d cannot be seen in this kind of QSAR studies, since basic force-field based molecular interaction fields are used. However, for structure–activity relationships these interaction fields have proven their usefulness.

A combination of a blue and red surface region near the 3-carbonyl-like groups can be explained by ester functionalities of highly potent DHPs where the alkoxy oxygen is close to the red surface. In contrast, molecules containing a lactam or lactone (*e.g.*, **46** and **47**) show low inhibition activity and are surrounded by a blue surface. The electronegative charge of the carbonyl group negatively correlates with inhibition activity which is represented by the electropositive surface nearby. Similarly, the nitrile group of **19** lies also within this area.

The steric contour map in Fig. 4c shows a green surface around the distal 4'-substituent which implies that sterically demanding groups are well-tolerated and correlate positively with activity. This is supported by DHPs with either a lack of 4'-substituents (*e.g.*, **S1**, **S2**, **S5**–**S6**, **8***, **S8**) or small substituents in 4'-position (*e.g.*, **7***, **S3**, **S4**) that show a low inhibition. In contrast, the yellow surface above the DHP core indicates areas which should not be covered with substituents. Such compounds were for example 3'-aryl-substituted DHPs (**39***, **40***–**43***) that were inactive or had a low potency. Although, among the most potent molecules, the contour map does not indicate steric or electrostatic surfaces for 7-substituted DHPs (*e.g.*, **25***, **29***, **28***). In this regard, more DHP derivatives of this kind would have to be experimentally evaluated to allow for more detailed QSAR conclusions or meaningful predictions, respectively.

Together, the initial qualitative SAR features that were manually extracted can be transferred into quantitative structure activity relationships. This supports the assumption that a distinct target within the TGFβ pathway is addressed by these DHPs, and that rather "unspecific" effects such as biological activity as a simple function of cell permeability contribute (at least) to a minor extent. In fact, this is further substantiated by plotting calculated logP (clogP) values versus inhibition activity (Fig. 4d): There is a certain trend indicating that the most potent compounds are also the most lipophilic and the inactive ones are very hydrophilic. This observation makes sense considering that compounds would have to enter the cells to exert principal cellular activity. However, there is clearly no good correlation between clogP and biological activity that does not allow discriminating weakly from strongly potent DHPs (*i.e.*, in the range between 20 and 100% inhibition, red rectangle).

3. Conclusion

Targeting the TGFβ pathway is an attractive pharmacological strategy for several therapeutic applications given its role as a key player in many pathologies, including cancer, autoimmune diseases and fibrosis. The herein presented subclass of *b*-annelated 1,4-dihydropyridines represent promising novel pharmacological tools since they interfere with TGFβ/Smad signaling in an unprecedented fashion, namely through induction of TGFβ receptor type II degradation. Here, we reported on a substantial extension of the DHP's SAR profile as TGFβ inhibitors, particularly addressing the inclusion of more versatile substituted and functionalized derivatives.

More than 40 novel DHPs were synthesized via classic Hantzsch conditions using distinct β-dicarbonyl and acetylenedicarboxylate building blocks coupled with Suzuki cross coupling and allowed the construction of the majority of the desired compounds. However, a synthetic route starting from 2-bromomethyl dihydropyridine **42** proved to be extremely useful to furnish miscellaneously functionalized DHPs.

Since no SAR information was present regarding the 2-position of these DHPs as TGFβ inhibitors, we tested several carboxylate, ether and amino functionalities for activity and found that quite a few groups are indeed well-tolerated (*e.g.*, 2-amino DHPs **40**, **41**, IC_{50}'s = 0.5–1.3 μM and *n*-propyl amine **45**, IC_{50} = 1.6 μM). It is thus tempting to speculate that the region surrounding the 2-position could possibly be solvent-exposed. Furthermore, exploration of the 3-position provided compelling evidence that a specific and important molecular interaction originates from this position. In particular H-bond acceptor properties, exemplified with simple ketones (*e.g.*, **14**, IC_{50} = 0.5 μM), together with a C_3–C_4 aliphatic, low-branched side chain defined the spatial and electronic requirements for this pharmacophoric region. An important objective in this study was also to provide a structural explanation of the significance of the 4-substituent which was evident from our previous work. Through thorough evaluation of series of distinct 4''-substituted DHPs we were able to show that pathway selectivity against TGFβ over Activin A was indeed dependent of the electronic nature of the 4''-substituent (Hammett constant). However, a small-sized electron withdrawing 4''-substituent, devoid of π-bonds, ensured highest degree of selectivity. Molecular electrostatic potential (MEP) calculations further shed light on this phenomenon. Against an intuitive expectation that electron-withdrawing substituents in 4''-position would generate an electron-deficient distal aromatic ring, MEP calculations suggested the opposite: The 4''-CF_3 group (**22**) creates an electron-rich distal aromatic by pulling electron density from the proximal 4-phenyl into the distal ring. Therefore, the distal 4'-region of the molecule is important for potent (and selective) interaction with the unknown cellular target.

Another key objective was to determine the − up to now − unknown absolute configuration of the active (+)-enantiomers by X-ray crystal structure analysis, which revealed an (R)-configuration at the DHPs center of chirality. Typical structural features of classic dihydropyridines were conserved for these *b*-annelated DHPs such as the flattened boat conformation and the pseudoaxial orientation of the 4-substituent, although in a more shallow dihedral angle (107°) as compared to similar DHPs.

Finally, the entire dataset was used to establish a 3D-QSAR model with the primary aim to further reinforce the selective nature of observed TGFβ inhibiting activity. Although based on cellular assay data the resulting model turned out to be robust ($r^2 = 0.93$) and exhibited a good predictive power ($r^2_{pred} = 0.69$). Therefore, it supports the hypothesis that these type of *b*-annelated 1,4-DHPs exert their novel TGFβ inhibitory mode of action through binding a distinct target and that unspecific activities that would derive from intrinsic properties of the ligands (*e.g.*, lipophilicity) play a negligible role.

In summary, the presented body of work not only provides compelling evidence that specific *b*-annelated DHPs address a distinct target or mechanism within TGFβ/Smad signaling but that the target appears "druggable". It also provides a solid basis for the further design of novel DHPs or DHP scaffold-derived compounds for rational hit-to-lead optimization required for more comprehensive pharmacological *in vivo* studies.

4. Experimental

4.1. Chemistry

4.1.1. General

Unless otherwise stated, all reagents were obtained from commercially available sources and were used without purification. The reaction process was monitored by TLC with silica gel plates (thickness 250 mm, Indicator F-254) under UV light. Flash column chromatography was performed on a CombiFlash Rf200 (Teledyne ISCO, Lincoln). Reactions under microwave irradiation were performed in a CEM, Discover Intellivent Explorer Automated Reactor. NMR spectra of compounds were recorded with a Varian Mercury BB (400 MHz) spectrometer, a Bruker DRX-400 spectrometer or a Bruker DRX-500 spectrometer. Chemical shifts were reported as ppm (δ) relative to the solvent (CDCl$_3$ at 7.26 ppm, DMSO-d$_6$ at 2.50 ppm) or TMS as internal standard. The coupling constants are expressed in Hertz (Hz). Multiplicities are abbreviated as s = singlet, d = doublet, t = triplet, q = quartet, sex = sextet, sep = septet, m = multiplet, br = broad. Mass spectral data were either determined on a Waters Acquity UPLC system connected to a Waters SQ Detector-2 operating in the ESI positive ion mode on a Waters Acquity UPLC® BEH C18 column (1.7 μm, 2.1 × 50 mm) using a gradient elution with acetonitrile (0.01% trifluoroacetic acid) in water (0.01% trifluoroacetic acid) at a flow rate of 0.4 mL/min or on a Agilent technologies 1200 system with Kinetex RP-18 (2.6 μm, 100 × 2.10 mm) using a gradient elution with acetonitrile (0.1% formic acid) and water (0.1% formic acid) at a flow rate of 0.25 mL/min, coupled to a Finnigan LCQ Advantage MAX ESI-spectrometer. Preparative HPLC purification was performed on a Shimadzu system (2 × LC-20 AP (pumps), SPD-20 AC XR (PDA-detector) with a Macherey–Nagel VarioPrep, Nucleodur C-18ec (5 μm, 250 × 21 mm). Purity of final compounds were either determined on a on a Agilent technologies 1200 system (Kinetex RP-18, 2.6 μm, 100 × 2.10 mm) using a gradient elution with acetonitrile (0.1% formic acid) and water (0.1% formic acid) at a flow rate of 0.25 mL/min over 18 min or on a Varian Star #1 (Apollo-C18, 150 × 4.6 mm Size) using a gradient elution with water (0.1% H$_3$PO$_4$) and acetonitrile (40/60 to 0/100, A/B) at a flow rate of 1.0 mL/min over

15 min. Purity of all synthetic final products was ≥95%.

4.1.2. Synthetic procedures for the preparation of 1,4-dihydropyidines *1, 6−21*

Procedure A. 1 eq. of a cyclic 1,3-dicarbonyl compound **2**, 1 eq. of the desired aldehyde **5**, 1 eq. of a 1,3-dicarbonyl compound **3**, 1 eq. of dried NH$_4$OAc and 0.3 eq. of iodine were stirred in EtOH (2.5 mL/mmol) overnight at room temperature. The solvent was evaporated and the residue was dissolved in EtOAc. The organic layer was washed twice with a saturated solution of NaS$_2$O$_3$ and brine, dried over MgSO$_4$ and concentrated under reduced pressure. The crude material was purified by recrystallization or flash chromatography.

Procedure B. 1 eq. of a cyclic 1,3-dicarbonyl compound **2**, 1 eq. of the desired aldehyde **5**, 1.2 eq. of a 1,3-dicarbonyl compound **3**, 1.5 eq. of dried NH$_4$OAc, 0.3 eq. of iodine and a few drops of concentrated acetic acid were stirred in EtOH (2.5 mL/mmol) under Ar at 60−80 °C. The progress of the reaction was monitored via TLC. Upon completion of the reaction the solvent was evaporated and the residue was dissolved in EtOAc. The organic layer was washed twice with a saturated NaS$_2$O$_3$ solution and brine, dried over MgSO$_4$ and concentrated under reduced pressure. The crude material was purified by recrystallization or flash chromatography.

4.1.3. Ethyl 4-(biphenyl-4-yl)-2,7,7-trimethyl-5-oxo-1,4,5,6,7,8-hexahydroquinoline-3-carboxylate (**1**)

The title compound was obtained according to the general procedure A using 4-biphenylcarboxaldehyde **33** as the aldehyde component, dimedone as the cyclic 1,3-dicarbonyl compound and ethyl acetoacetate as the 1,3-dicarbonyl compound. Yellow solid; yield: 38%. Analytical data are in accordance with the literature [8].

4.1.4. Ethyl 4-(4-bromophenyl)-2,7,7-trimethyl-5-oxo-1,4,5,6,7,8-hexahydroquinoline-3-carboxylate (**6**)

The title compound was obtained according to the general procedure A using 4-bromophenylcarboxaldehyde as the aldehyde component, dimedone as the cyclic 1,3-dicarbonyl compound and ethyl acetoacetate as the 1,3-dicarbonyl compound. Yellow solid; yield: 40%. TLC: R$_f$ = 0.38 (cyclohexane/EtOAc, 1:1). ^{1}H NMR (500 MHz, DMSO-d$_6$): δ = 9.01 (br s, 1H), 7.37 (m, 2H), 7.09 (m, 2H), 4.82 (s, 1H), 3.96 (q, J = 7.3 Hz, 2H), 2.40 (m, 1H), 2.29 (s, 3H), 2.27 (m, 1H), 2.16 (m, 1H), 1.98 (m, 1H), 1.11 (t, J = 7.3 Hz, 3H), 1.00 (s, 3H), 0.83 (s, 3H) ppm. MS (+ESI) *m/z*: 418.32 [M+H]$^+$.

4.1.5. Ethyl 4-(4-(4-bromophenyl)phenyl)-2,7,7-trimethyl-5-oxo-1,4,5,6,7,8-hexahydroquinoline-3-carboxylate (**7**)

The title compound was obtained according to the general procedure A using 4-bromobiphenylcarboxaldehyde as the aldehyde component, dimedone as the cyclic 1,3-dicarbonyl compound and ethyl acetoacetate as the 1,3-dicarbonyl compound. Yellow solid; yield: 38%. TLC: R$_f$ = 0.42 (cyclohexane/EtOAc, 1:1). ^{1}H NMR (500 MHz, DMSO-d$_6$): δ = 9.07 (br s, 1H), 7.58 (m, 4H), 7.49 (m, 2H), 7.24 (m, 2H), 4.89 (s, 1H), 3.99 (q, J = 7.1 Hz, 2H), 2.43 (m, 1H), 2.32 (m, 4H), 2.18 (m, 1H), 2.00 (m, 1H), 1.15 (t, J = 7.1 Hz, 3H), 1.00 (s, 3H), 0.86 (s, 3H) ppm. MS (+ESI) *m/z*: 494.20 [M+H]$^+$.

4.1.6. Ethyl 4-(4-ethynylphenyl)-2,7,7-trimethyl-5-oxo-1,4,5,6,7,8-hexahydroquinoline-3-carboxylate (**8**)

The title compound was obtained according to the general procedure A using 4-ethynylphenylcarboxaldehyde as the aldehyde component, dimedone as the cyclic 1,3-dicarbonyl compound and ethyl acetoacetate as the 1,3-dicarbonyl compound. Yellow solid; yield: 37%. TLC: R$_f$ = 0.46 (cyclohexane/EtOAc, 1:1). ^{1}H NMR (500 MHz, DMSO-d$_6$): δ = 9.08 (br s, 1H), 7.30 (m, 2H), 7.15 (m, 2H), 4.85 (s, 1H), 4.03 (s, 1H), 3.96 (q, J = 7.3 Hz, 2H), 2.41 (d, J = 16.8 Hz,

1H), 2.29 (s, 3H), 2.27 (d, J = 16.1 Hz, 1H), 2.16 (d, J = 16.1 Hz, 1H), 1.97 (d, J = 16.1 Hz, 1H), 1.11 (t, J = 7.3 Hz, 3H), 1.00 (s, 3H), 0.83 (s, 3H) ppm. MS (+ESI) m/z: 346.03 [M+H]$^+$.

4.1.7. 4-(Biphenyl-4-yl)-2,7,7-trimethyl-5-oxo-1,4,5,6,7,8-hexahydroquinoline-3-carboxylic acid ethylamide (9)

The title compound was obtained according to the general procedure A using 4-biphenylcarboxaldehyde as the aldehyde component, dimedone as the cyclic 1,3-dicarbonyl compound and *N*-ethyl-3-oxo-butanamide as the 1,3-dicarbonyl compound. Yellow solid; yield: 17%. TLC: R_f = 0.25 (cyclohexane/EtOAc, 1:3). ^{1}H NMR (500 MHz, DMSO-d$_6$): δ = 8.56 (br s, 1H), 7.59 (m, 2H), 7.47 (m, 2H), 7.42 (m, 2H), 7.31 (m, 1H), 7.23 (m, 2H), 4.85 (s, 1H), 3.04 (m, 2H), 2.38 (m, 1H), 2.30 (m, 1H), 2.14 (m, 1H), 2.03 (s, 3H), 1.99 (m, 1H), 1.02 (s, 3H), 0.93 (t, J = 7.3 Hz, 3H), 0.91 (s, 3H) ppm. MS (+ESI) m/z: 415.01 [M+H]$^+$.

4.1.8. t-Butyl 4-(biphenyl-4-yl)-2,7,7-trimethyl-5-oxo-1,4,5,6,7,8-hexahydroquinoline-3-carboxylate (10)

The title compound was obtained according to the general procedure A using 4-biphenylcarboxaldehyde as the aldehyde component, dimedone as the cyclic 1,3-dicarbonyl compound and *t*-butyl acetoacetate as the 1,3-dicarbonyl compound. Yellow solid; yield: 33%. TLC: R_f = 0.18 (cyclohexane/EtOAc, 2:1). ^{1}H NMR (500 MHz, DMSO-d$_6$): δ = 8.99 (br s, 1H), 7.60 (m, 2H), 7.50 (m, 2H), 7.42 (m, 2H), 7.31 (m, 1H), 7.24 (m, 2H), 4.82 (s, 1H), 2.41 (m, 1H), 2.30 (m, 1H), 2.26 (s, 3H), 2.16 (m, 1H), 1.98 (m, 1H), 1.33 (s, 9H), 1.01 (s, 3H), 0.87 (s, 3H) ppm. MS (+ESI) m/z: 444.13 [M+H]$^+$.

4.1.9. Allyl 4-(biphenyl-4-yl)-2,7,7-trimethyl-5-oxo-1,4,5,6,7,8-hexahydroquinoline-3-carboxylate (11)

The title compound was obtained according to the general procedure A using 4-biphenylcarboxaldehyde as the aldehyde component, dimedone as the cyclic 1,3-dicarbonyl compound and allyl acetoacetate as the 1,3-dicarbonyl compound. Yellow solid; yield: 23%. TLC: R_f = 0.19 (cyclohexane/EtOAc, 2:1). ^{1}H NMR (400 MHz, CDCl$_3$): δ = 7.56 (m, 2H), 7.43 (m, 6H), 7.31 (m, 1H), 6.19 (br s, 1H), 5.88 (m, 1H), 5.18 (m, 3H), 4.57 (d, J = 5.3 Hz, 2H), 2,42 (s, 3H), 2.37 (m, 1H), 2.25 (m, 1H), 2.24 (m, 1H), 2.19 (m, 1H), 1.10 (s, 3H), 0.97 (s, 3H) ppm. MS (+ESI) m/z: 427.96 [M+H]$^+$.

4.1.10. Ethyl 4-(biphenyl-4-yl)-2-methyl-5-oxo-1,4,5,6,7,8-hexahydro-[1,6]naphthyridine-3-carboxylate (12)

The title compound was obtained according to the general procedure B using 4-biphenylcarboxaldehyde as the aldehyde component, piperidine-2,4-dione as the cyclic 1,3-dicarbonyl compound and ethyl acetoacetate as the 1,3-dicarbonyl compound. The reaction was completed after 72 h. Colorless solid; yield: 36%. TLC: R_f = 0.57 (chloroform/hexane/acetone/methanol, 10:5:2:1). ^{1}H NMR (400 MHz, CDCl$_3$): δ = 8.06 (br s, 1H), 7.44 (m, 4H), 7.32 (m, 4H), 7.20 (m, 1H), 5.70 (s, 1H), 5.02 (s, 1H), 3.95 (q, J = 7.1 Hz, 2H), 3.26 (m, 2H), 2.75 (br s, 2H), 2.28 (s, 3H), 1.11 (t, J = 7.1 Hz, 3H) ppm. MS (+ESI) m/z: 389 [M+H]$^+$.

4.1.11. Dodecyl 4-(biphenyl-4-yl)-2,7,7-trimethyl-5-oxo-1,4,5,6,7,8-hexahydroquinoline-3-carboxyate (13)

The title compound was obtained according to the general procedure B using 4-biphenylcarboxaldehyde as the aldehyde component, dimedone as the cyclic 1,3-dicarbonyl compound and dodecyl 3-oxo-butanoate as the 1,3-dicarbonyl compound. Yield: 395 mg (71%) as white powder, mp 170 °C; TLC: R_f = 0.69 (hexane/EtOAc, 1:1); ^{1}H NMR (400 MHz, CDCl$_3$): δ = 7.54 (m, 2H), 7.43 (m, 2H), 7.38 (m, 4H), 7.28 (m, 1H), 6.45 (s, 1H), 5.10 (s, 1H), 4.02 (m, 2H), 2.39 (s, 3H), 2.24 (m, 4H), 1.57 (m, 2H), 1.20 (br s, 18H), 1.06 (s, 3H), 0.93 (s, 3H), 0.88 (t, J = 8.0 Hz, 3H) ppm. MS (+ESI) m/z: 556

[M+H]$^+$.

4.1.12. 4-(Biphenyl-4-yl)-3-butyryl-2,7,7-trimethyl-5-oxo-1,4,5,6,7,8-hexahydroquinoline (14)

The title compound was obtained according to the general procedure B using 4-biphenylcarboxaldehyde as the aldehyde component, dimedone as the cyclic 1,3-dicarbonyl compound and heptane-2,4-dioneas the 1,3-dicarbonyl compound. Yellow solid; yield: 55%. TLC: R_f = 0.39 (hexane/EtOAc, 1:1). 1H NMR (400 MHz, CDCl$_3$): δ = 7.53 (m, 2H), 7.46 (m, 2H), 7.38 (m, 4H), 7.30 (m, 1H), 6.09 (br s, 1H), 5.18 (s, 1H), 2.62 (m, 1H), 2.40 (s, 3H), 2.31 (m, 3H), 2.20 (m, 2H), 1.53 (m, 2H), 1.07 (s, 3H), 0.88 (s, 3H), 0.82 (t, J = 7.2 Hz, 3H) ppm. MS (+ESI) m/z: 414 [M+H]$^+$.

4.1.13. 4-(Biphenyl-4-yl)-2,7,7-trimethyl-3-pentanoyl-5-oxo-1,4,5,6,7,8-hexahydroquinoline (15)

The title compound was obtained according to the general procedure B using 4-biphenylcarboxaldehyde as the aldehyde component, dimedone as the cyclic 1,3-dicarbonyl compound and octane-2,4-dione as the 1,3-dicarbonyl compound. Colorless solid; yield: 21%. TLC: R_f = 0.50 (hexane/EtOAc, 1:1). ^{1}H NMR (400 MHz, CDCl$_3$): δ = 7.54 (m, 2H), 7.46 (m, 2H), 7.38 (m, 4H), 7.30 (m, 1H), 5.80 (br s, 1H), 5.17 (s, 1H), 2.40 (s, 3H), 2.30 (m, 4H), 2.18 (m, 2H), 1.45 (m, 2H), 1.23 (m, 2H), 1.08 (s, 3H), 0.88 (s, 3H), 0.82 (t, J = 7.3 Hz, 3H) ppm. MS (+ESI) m/z: 428 [M+H]$^+$.

4.1.14. 4-(Biphenyl-4-yl)-7,7-dimethyl-2-ethyl-3-propionyl-5-oxo-1,4,5,6,7,8-hexahydroquinoline (16)

The title compound was obtained according to the general procedure B using 4-biphenylcarboxaldehyde as the aldehyde component, dimedone as the cyclic 1,3-dicarbonyl compound and heptane-3,5-dione as the 1,3-dicarbonyl compound. Colorless solid; yield: 31%. TLC: R_f = 0.40 (hexane/EtOAc, 1:1). ^{1}H NMR (400 MHz, CDCl$_3$): δ = 7.49 (m, 4H), 7.34 (m, 5H), 5.74 (br s, 1H), 5.17 (s, 1H), 2.86 (m, 1H), 2.68 (m, 2H), 2.29 (m, 5H), 1.29 (t, J = 7.6 Hz, 3H), 1.07 (s, 3H), 0.95 (t, J = 7.2 Hz, 3H), 0.86 (s, 3H) ppm. MS (+ESI) m/z: 414 [M+H]$^+$.

4.1.15. 4-(Biphenyl-4-yl)-2,7,7-trimethyl-5-oxo-1,4,5,6,7,8-hexahydroquinoline-3-carboxylic acid benzylamide (17)

The title compound was obtained according to the general procedure B using 4-biphenylcarboxaldehyde as the aldehyde component, dimedone as the cyclic 1,3-dicarbonyl compound and *N*-benzyl-3-oxopentanamide as the 1,3-dicarbonyl compound. Light yellow solid; yield: 68%. TLC: R_f = 0.50 (PE/EtOH, 1:1). ^{1}H NMR (400 MHz, CDCl$_3$): δ = 7.54 (m, 2H), 7.46 (m, 2H), 7.40 (m, 4H), 7.33 (m, 1H), 7.20 (m, 3H), 7.00 (m, 2H), 5.85 (t, J = 4.8 Hz, 1H), 5.71 (s, 1H), 4.88 (s, 1H), 4.39 (m, 4H), 2.40 (s, 3H), 2.24 (m, 4H), 1.08 (s, 3H), 0.91 (s, 3H) ppm. MS (+ESI) m/z: 477 [M+H]$^+$.

4.1.16. 2-Propoxyethyl 4-(biphenyl-4-yl)-2,7,7-trimethyl-5-oxo-1,4,5,6,7,8-hexahydroquinoline-3-carboxylate (18)

The title compound was obtained according to the general procedure B using 4-biphenylcarboxaldehyde as the aldehyde component, dimedone as the cyclic 1,3-dicarbonyl compound and propoxyethyl 3-oxobutanoate as the 1,3-dicarbonyl compound. Yellow solid; yield: 67%. TLC: R_f = 0.52 (hexane/EtOH, 1:1). ^{1}H NMR (400 MHz, CDCl$_3$): δ = 7.51 (m, 2H), 7.41 (m, 2H), 7.36 (m, 4H), 7.27 (m, 1H), 6.12 (br s, 1H), 5.11 (s, 1H), 4.16 (m, 2H), 3.56 (t, J = 5.2 Hz, 2H), 3.35 (m, 2H), 2.37 (s, 3H), 2.22 (m, 4H), 1.55 (m, 2H), 1.06 (s, 3H), 0.93 (s, 3H), 0.87 (t, J = 7.2 Hz, 3H) ppm. MS (+ESI) m/z: 474 [M+H]$^+$.

4.1.17. Dimethyl 4-(biphenyl-4-yl)-7,7-dimethyl-5-oxo-1,4,5,6,7,8-hexahydroquinoline-2,3-dicarboxylate (20)

The title compound was obtained according to the general procedure B using 4-biphenylcarboxaldehyde as the aldehyde component, dimedone as the cyclic 1,3-dicarbonyl compound, but-2-ynedioic acid dimethyl ester as the 1,3-dicarbonyl compound and methanol as the solvent. Colorless solid; yield: 42%. TLC: R_f = 0.49 (hexane/EtOAc, 1:1). ^{1}H NMR (400 MHz, CDCl$_3$): δ = 7.54 (m, 2H), 7.47 (m, 2H), 7.37 (m, 4H), 7.29 (m, 1H), 6.47 (br s, 1H), 5.00 (s, 1H), 3.85 (s, 3H), 3.65 (s, 3H), 2.35 (m, 2H), 2.22 (m, 2H), 1.09 (s, 3H), 0.98 (s, 3H) ppm. MS (+ESI) m/z: 446 [M+H]$^+$.

4.1.18. Diethyl 4-(biphenyl-4-yl)-7,7-dimethyl-5-oxo-1,4,5,6,7,8-hexahydroquinoline-2,3-dicarboxylate (21)

The title compound was obtained according to the general procedure B using 4-biphenylcarboxaldehyde as the aldehyde component, dimedone as the cyclic 1,3-dicarbonyl compound and but-2-ynedioic acid diethyl ester as the 1,3-dicarbonyl compound. Colorless solid; yield: 53%. TLC: R_f = 0.69 (hexane/EtOAc, 1:1). ^{1}H NMR (400 MHz, CDCl$_3$): δ 7.54 (m, 2H), 7.48 (m, 2H), 7.38 (m, 4H), 7.29 (m, 1H), 6.61 (br s, 1H), 4.99 (s, 1H), 4.30 (m, 2H), 4.11 (m, 2H), 2.35 (m, 2H), 2.21 (m, 2H), 1.31 (t, J = 7.2 Hz, 3H), 1.15 (t, J = 7.2 Hz, 3H), 1.09 (s, 3H), 0.99 (s, 3H) ppm. MS (+ESI) m/z: 474 [M+H]$^+$.

4.1.19. 4-(Biphenyl-4-yl)-2,7,7-trimethyl-5-oxo-1,4,5,6,7,8-hexahydroquinoline-3-carbonitrile (19)

A solution consisting of 1 eq. of dimedone, 1 eq. of 4-biphenylcarboxaldehyde and 1 eq. of β-aminocrotonitrile in ethanol (2.5 mL/mmol) was refluxed for 1.5 h. After cooling the precipitate was filtered and washed with cold ethanol (1 mL/mmol). The solid was suspended in hot ethanol and filtered. The filtrate was evaporated to dryness and recrystallized from ethanol. Colorless solid; yield: 33%. TLC: R_f = 0.25 (hexane/EtOAc, 1:1). ^{1}H NMR (400 MHz, DMSO-d$_6$): δ = 9.46 (br s, 1H), 7.62 (m, 2H), 7.57 (m, 2H), 7.48 (m, 2H), 7.34 (m, 1H), 7.26 (m, 2H), 4.46 (s, 1H), 2.43 (m, 1H), 2.36 (m, 1H), 2.19 (m, 1H), 2.07 (s, 3H), 2.03 (m, 1H), 1.02 (s, 3H), 0.94 (s, 3H) ppm. MS (+ESI) m/z: 369 [M+H]$^+$.

4.1.20. 3-Methyl 4-(biphenyl-4-yl)-7,7-dimethyl-5-oxo-1,4,5,6,7,8-hexahydroquinoline-2,3-dicarboxylate (20a)

A solution of 1 eq. dimethyl 4-(biphenyl-4-yl)-7,7-dimethyl-5-oxo-1,4,5,6,7,8-hexahydroquinoline-2,3-dicarboxylate (20) in methanol (8 mL/mmol) was added to a sodium hydroxide solution (3 eq. in 0.34 mL/mmol water). The mixture was stirred at room temperature for 5 h. The excess of methanol was removed in vacuo. The residue was dissolved in water (6 mL/mmol), filtered and cooled in ice bath. The mixture was acidified with diluted hydrochloric acid until precipitation occurred. The solid was filtered, washed with water and recrystallized from EtOAc. Light yellow solid; yield: 68%. TLC: R_f = 0.44 (DCM/methanol, 1:1) ^{1}H NMR (400 MHz, DMSO-d$_6$): δ = 9.75 (s, 1H), 7.61 (m, 2H), 7.53 (d, J = 8.2 Hz, 2H), 7.43 (t, J = 8.2 Hz, 2H), 7.32 (m, 1H), 7.25 (d, J = 8.2 Hz, 2H), 4.86 (s, 1H), 3.55 (s, 3H), 2.41 (m, 2H), 2.22 (m, 1H), 2.01 (m, 1H), 1.01 (s, 3H), 0.87 (s, 3H) ppm. MS (+ESI) m/z: 432 [M+H]$^+$.

4.1.21. 3-Ethyl 4-(biphenyl-4-yl)-7,7-dimethyl-5-oxo-1,4,5,6,7,8-hexahydroquinoline-2,3-dicarboxylate (21a)

A solution of 1 eq. diethyl 4-(biphenyl-4-yl)-7,7-dimethyl-5-oxo-1,4,5,6,7,8-hexahydroquinoline-2,3-dicarboxylate (21) in ethanol (8 mL/mmol) was added to a sodium hydroxide solution (3 eq. in 0.34 mL/mmol water). The mixture was stirred at room temperature for 5 h. The excess of methanol was removed in vacuo. The residue was dissolved in water (6 mL/mmol), filtered and cooled in ice bath. The mixture was acidified with diluted hydrochloric acid until precipitation occurred. The solid was filtered, washed with water and recrystallized from EtOAc. Light yellow solid; yield: 87%. TLC: R_f = 0.44 (DCM/methanol, 1:1). ^{1}H NMR (400 MHz, DMSO-d$_6$): δ = 9.77 (s, 1H), 7.54 (m, 2H), 7.47 (m, 2H), 7.41 (m, 2H), 7.33 (m, 3H), 5.30 (s, 1H), 4.31 (q, J = 7.2 Hz, 2H), 2.41 (m, 2H), 2.26 (m, 2H), 1.34 (t, J = 7.2 Hz, 3H), 1.11 (s, 3H), 0.97 (s, 3H) ppm. MS (+ESI) m/z: 446 [M+H]$^+$.

4.1.22. 2-Benzyl-9-(biphenyl-4-yl)-6,6-dimethyl-2,3,5,6,7,9-hexahydro-4H-pyrrolo[3,4-b]quinolone-1,8-dione (55)

To a stirred solution of 1 eq. 4-(biphenyl-4-yl)-2,7,7-trimethyl-5-oxo-1,4,5,6,7,8-hexahydroquinoline-3-carboxylic acid benzylamide (17) in methanol (60 mL/mmol) was added 1.1 eq. NBS at 0 °C. After completion of the addition, the mixture was stirred for 24 h at room temperature. The reaction was monitored via TLC. After completion of the reaction the solvent was evaporated and the residue was washed with sat. NaHCO$_3$ solution and water. The remaining solid was dried and recrystallized from methanol. Colorless solid; yield: 81%. TLC: R_f = 0.26 (hexanes/EtOAc, 1:1). ^{1}H NMR (400 MHz, DMSO-d$_6$): δ = 9.71 (br s, 1H), 7.60 (m, 2H), 7.51 (m, 2H), 7.43 (m, 2H), 7.34 (m, 3H), 7.16 (m, 5H), 4.96 (m, 1H), 4.89 (m, 1H), 4.76 (s, 1H), 4.43 (m, 2H), 2.47 (m, 2H), 2.14 (m, 2H), 1.04 (s, 3H), 1.00 (s, 3H) ppm. MS (+ESI) m/z: 475 [M+H]$^+$.

4.1.23. 4-(Biphenyl-4-yl)-2-bromomethyl-7,7-dimethyl-3-ethoxycarbonyl-5-oxo-1,4,5,6,7,8-hexahydroquinoline (42)

To a stirred solution of 1 eq. of ethyl 4-(biphenyl-4-yl)-2-methyl-7,7-dimethyl-5-oxo-1,4,5,6,7,8-hexahydroquinoline-3-carboxylate (1) in MeOH (50 mL/mmol) was added 1.05 eq. of NBS portionwise at 0 °C. The mixture was stirred at r.t. for 3 days. The solvent was evaporated under reduced pressure and residue was triturated with water. The yellow precipitate was filtered, dried and purified by flash chromatography (PE/EtOAc, 1:1). Bright yellow solid; yield: 51%. TLC: R_f = 0.63 (hexanes/EtOAc, 1:1). ^{1}H NMR (400 MHz, CDCl$_3$): δ = 7.34 (m, 2H), 7.27 (m, 2H), 7.20 (m, 4H), 7.10 (m, 1H), 6.75 (br s, 1H), 4.94 (s, 1H), 4.57 (m, 2H), 3.94 (q, J = 7.2 Hz, 2H), 2.13 (m, 4H), 1.05 (t, J = 7.2 Hz, 3H), 0.91 (s, 3H), 0.78 (s, 3H) ppm. MS (+ESI) m/z: 495 [M+H]$^+$.

4.1.24. Ethyl 4-(biphenyl-4-yl)-2-methoxymethyl-7,7-dimethyl-5-oxo-1,4,5,6,7,8-hexahydroquinoline-3-carboxylate (48)

To a stirred mixture of 1 eq. ethyl 4-(biphenyl-4-yl)-2-bromomethyl-7,7-dimethyl-5-oxo-1,4,5,6,7,8-hexahydroquinoline-3-carboxylate (42) in DMF (4 mL/mmol) 2 eq. of potassium hydroxide in water (1.25 mL/mmol) was added at 0 °C. After stirring at r.t. for 24 h, water was added and the pH was adjusted to neutral with diluted hydrochloric acid. The precipitate was filtered and recrystallized from methanol. Colorless solid; yield: 91%. TLC: R_f = 0.68 (hexanes/EtOAc, 1:1). ^{1}H NMR (400 MHz, CDCl$_3$): δ = 7.54 (m, 2H), 7.43 (m, 2H), 7.38 (m, 3H), 7.29 (m, 2H), 7.16 (br s, 1H), 5.10 (s, 1H), 4.75 (m, 1H), 4.70 (m, 1H), 4.07 (m, 2H), 3.50 (s, 3H), 2.36 (m, 2H), 2.23 (m, 2H), 1.20 (t, J = 7.2 Hz, 3H), 1.10 (s, 3H), 0.98 (s, 3H) ppm. MS (+ESI) m/z: 446 [M+H]$^+$.

4.1.25. Ethyl 4-(biphenyl-4-yl)-2-ethylaminomethyl-7,7-dimethyl-5-oxo-1,4,5,6,7,8-hexahydroquinoline-3-carboxylate hydrochloride (44)

3 eq. Ethylamine (70% solution in water) was added to a stirred solution of 1 eq. ethyl 4-(biphenyl-4-yl)-2-bromomethyl-7,7-dimethyl-5-oxo-1,4,5,6,7,8-hexahydroquinoline-3-carboxylate (42) in DCM (4 mL/mmol) and DMF (0.2 mL/mmol) at 0 °C under argon. After 30 min the reaction was warmed to room temperature and stirred for 24 h. The solvents were evaporated to under reduced pressure. The residue was taken up with DCM (20 mL/mmol) and the organic layer was washed with water, dried over Na$_2$SO$_4$ and

evaporated. The crude product was purified by adding dry Et$_2$O (2 mL/mmol) and a few drops of concentrated hydrochloric acid at −10 °C. The precipitate was collected, washed with three small portions of dry Et$_2$O and recrystallized from MeOH. Light yellow solid; yield: 58%. ^{1}H NMR (400 MHz, DMSO-d$_6$): δ = 9.55 (s, 2H), 9.24 (br s, 1H), 7.53 (m, 2H), 7.48 (m, 2H), 7.39 (m, 4H), 7.30 (m, 1H), 5.09 (s, 1H), 4.61 (m, 1H), 4.36 (m, 1H), 3.23 (m, 2H), 2.60 (m, 1H), 2.54 (m, 1H), 2.21 (m, 2H), 1.47 (t, J = 7.2 Hz, 3H), 1.28 (t, J = 7.2 Hz, 3H), 1.09 (s, 3H), 0.95 (s, 3H) ppm. MS (+ESI) m/z: 459 [M+H]$^+$.

4.1.26. Ethyl 4-(biphenyl-4-yl)-7,7-dimethyl-2-propylaminomethyl-5-oxo-1,4,5,6,7,8-hexahydroquinoline-3-carboxylate hydrochlroride (45)

3 eq. *n*-Propyl amine was added to a stirred solution of 1 eq. ethyl 4-(biphenyl-4-yl)-2-bromomethyl-7,7-dimethyl-5-oxo-1,4,5,6,7,8-hexahydroquinoline-3-carboxylate (42) in DCM (4 mL/mmol) and DMF (0.2 mL/mmol) at 0 °C under argon. After 30 min the reaction was warmed to room temperature and stirred for 24 h. The solvents were evaporated to under reduced pressure. The residue was taken up with DCM (20 mL/mmol) and the organic layer was washed with water, dried over Na$_2$SO$_4$ and evaporated. The crude product was purified by adding dry Et$_2$O (2 mL/mmol) and a few drops of concentrated hydrochloric acid at −10 °C. The precipitate was collected, washed with three small portions of dry Et$_2$O and recrystallized from MeOH. Colorless solid; yield: 42%. ^{1}H NMR (400 MHz, CDCl3): δ = 9.56 (s, 2H), 9.12 (s, 1H), 7.52 (m, 2H), 7.44 (m, 2H), 7.37 (m, 4H), 7.30 (m, 1H), 5.09 (s, 1H), 4.59 (m, 1H), 4.34 (m, 1H), 4.14 (m, 2H), 3.08 (m, 2H), 2.55 (m, 2H), 2.21 (m, 2H), 1.86 (m, 2H), 1.28 (t, J = 7.2 Hz, 3H), 1.09 (s, 3H), 0.99 (m, 6H) ppm. MS (+ESI) m/z: 473 [M+H]$^+$.

4.1.27. 9-(Biphenyl-4-yl)-2-ethyl-6,6-dimethyl-2,3,5,6,7,9-hexahydro-4H-pyrrolo[3,4-b]quinoline-1,8-dione (46)

A 3 M potassium hydroxide solution (0.2 mL/mmol) was added to a stirred solution of 1 eq. of ethyl 4-(biphenyl-4-yl)-2-ethylaminomethyl-7,7-dimethyl-5-oxo-1,4,5,6,7,8-hexahydroquinoline-3-carboxylate hydrochloride (44) in EtOH (2 mL) at r.t. After stirring overnight the solvent was removed under reduced pressure. The residue was triturated with water and the precipitate was filtered and crystallized from MeOH. The crude product was purified by flash chromatography (chloroform/hexane/acetone/methanol: 9:7:2:1). Light yellow solid; yield: 59%. TLC: R$_f$ = 0.41 (chloroform/hexane/acetone/methanol, 9:7:2:1). ^{1}H NMR (400 MHz, DMSO-d$_6$): δ = 9.75 (br s, 1H), 7.59 (m, 2H), 7.49 (m, 2H), 7.42 (m, 2H), 7.32 (m, 1H), 7.25 (m, 2H), 4.70 (s, 1H), 4.06 and 3.96 (2 × d, AB-system, ^2J = 18 Hz, 2H), 3.31 (m, 2H), 2.44 (s, 2H), 2.12 (m, 2H), 1.02 (m, 9H) ppm. MS (+ESI) m/z: 413 [M+H]$^+$.

4.1.28. 9-(Biphenyl-4-yl)-6,6-dimethyl-5,6,7,9-tetrahydro-3H,4H-furo[3,4-b]quinoline-1,8-dione (47)

A solution of 1 eq. of ethyl 4-(biphenyl-4-yl)-2-bromomethyl-7,7-dimethyl-5-oxo-1,4,5,6,7,8-hexahydroquinoline-3-carboxylate (42) and 0.5 eq. potassium hydroxide in chloroform (10 mL/mmol) was refluxed for 3 h and evaporated to dryness. The residue was triturated with methanol (10 mL/mmol) and the precipitate was filtered and recrystallized from methanol. Colorless solid; yield: 80%. TLC: R$_f$ = 0.41 (chloroform/hexane/acetone/methanol, 9:7:1:1). ^{1}H NMR (400 MHz, DMSO-d$_6$): δ = 10.06 (br s, 1H), 7.61 (m, 2H), 7.52 (m, 2H), 7.44 (m, 2H), 7.33 (m, 1H), 7.27 (m, 2H), 4.95 (m, 1H), 4.86 (m, 1H), 4.68 (s, 1H), 2.47 (s, 2H), 2.16 (m, 2H), 1.04 (s, 3H), 0.99 (s, 3H) ppm. MS (+ESI) m/z: 386 [M+H]$^+$.

4.1.29. 9-(Biphenyl-4-yl)-6,6-dimethyl-2,3,5,6,7,9-hexahydro-4H-pyrrolo[3,4-b]quinoline-1,8-dione (43)

1 eq. Potassium phthalimide was added to a stirred solution of

1 eq. of ethyl 4-(biphenyl-4-yl)-2-bromomethyl-7,7-dimethyl-5-oxo-1,4,5,6,7,8-hexahydroquinoline-3 carboxylate (42) in DMF (3 mL/mmol) at 0 °C. After stirring the mixture at room temperature for 24 h the solvent was removed *in vacuo* and residue was purified by column chromatography (chloroform/hexane/acetone/methanol, 9:7:1:1) to give a yellow oil. This oil was dissolved in methanol (2 mL/mmol) and an excess of methylamine (20 eq.) was added to the solution. After stirring for 24 h the solvent was evaporated and the residue was purified by flash chromatography (chloroform/hexane/acetone/methanol, 10:5:2:1). Colorless solid; yield: 22% (2 steps). TLC: R$_f$ = 0.15 (chloroform/hexane/acetone/methanol, 10:5:2:1). ^{1}H NMR (400 MHz, DMSO-d$_6$): δ = 9.65 (br s, 1H), 7.59 (m, 2H), 7.49 (m, 2H), 7.43 (m, 3H), 7.32 (m, 1H), 7.26 (m, 2H), 4.70 (s, 1H), 3.98 and 2.88 (2 × d, AB-system, ^2J = 18.0 Hz, 2H), 2.43 (d, J = 5.2 Hz, 2H), 2.19 (m, 1H), 2.06 (m, 1H), 1.03 (s, 3H), 0.98 (s, 3H) ppm. MS (+ESI) m/z: 385 [M+H]$^+$.

4.1.30. 4-(Biphenyl-4-yl)-2,7,7-trimethyl-5-oxo-1,4,5,6,7,8-hexahydroquinoline-3-carboxylate (49)

To a cooled solution of 1 eq. of ethyl 4-(biphenyl-4-yl)-2,7,7-trimethyl-5-oxo-1,4,5,6,7,8-hexahydroquinoline-3-carboxylate (1) in dry DCM (8 mL/mmol) 4 eq. of a BCl$_3$-solution (1 M in DCM) was added. Then the mixture was stirred at room temperature overnight and diluted in ice water/EtOAc. The organic layer was dried over MgSO$_4$ and concentrated. The crude product was purified by flash chromatography with (DCM/MeOH, 95:5). Colorless solid; yield: 75%. Analytical data are in accordance with the literature [1].

4.1.31. General procedure for the alkylation of the carboxylic acid

1 eq. of 4-(biphenyl-4-yl)-2,7,7-trimethyl-5-oxo-1,4,5,6,7,8-hexahydroquinoline-3-carboxylate (49), 1.16 eq. of K$_2$CO$_3$, and 1.16 eq. of an alkyl bromide was stirred in dry DMF (30 mL/mmol) overnight at room temperature. For workup, water (150 mL/mmol) was added and the mixture was extracted with EtOAc. The combined organic layer was washed with water and brine, dried (MgSO$_4$), and concentrated to dryness. The crude mixture was purified by flash chromatography (cyclohexane/EtOAc, 1:1).

4.1.32. n-Propyl 4-(biphenyl-4-yl)-2,7,7-trimethyl-5-oxo-1,4,5,6,7,8-hexahydroquinoline-3-carboxylate (50)

The title compound was obtained according to the general procedure using *n*-propyl bromide as the alkylation reagent. Yellow solid; yield: 37%. TLC: R$_f$ = 0.23 (cyclohexane/EtOAc, 2:1). ^{1}H NMR (400 MHz, DMSO-d$_6$): δ = 9.12 (br s, 1H), 7.59 (m, 2H), 7.48 (m, 2H), 7.42 (m, 2H), 7.31 (m, 1H), 7.24 (m, 2H), 4.90 (s, 1H), 3.90 (m, 2H), 2.43 (m, 1H), 2.31 (s, 3H), 2.30 (m, 1H), 2.18 (m, 1H), 1.99 (m, 1H), (sxt, J = 7.0 Hz, 2H), 1.01 (s, 3H), 0.85 (s, 3H), 0.80 (t, J = 7.4 Hz, 3H) ppm. MS (+ESI) m/z: 429.99 [M+H]$^+$.

4.1.33. i-Propyl 4-(biphenyl-4-yl)-2,7,7-trimethyl-5-oxo-1,4,5,6,7,8-hexahydroquinoline-3-carboxylate (51)

The title compound was obtained according to the general procedure using *i*-propyl bromide as the alkylation reagent. Yellow solid; yield: 22%. TLC: R$_f$ = 0.26 (cyclohexane/EtOAc, 2:1). ^{1}H NMR (400 MHz, DMSO-d$_6$): δ = 9.08 (br s, 1H), 7.59 (m, 2H), 7.48 (m, 2H), 7.41 (m, 2H), 7.31 (m, 1H), 7.23 (m, 2H), 4.86 (s, 1H), 4.80 (sept, J = 6.3 Hz, 1H), 2.43 (m, 1H), 2.29 (s, 3H), 2.31 (m, 1H), 2.17 (m, 1H), 1.99 (m, 1H), 1.18 (d, J = 6.3 Hz, 3H), 1.06 (d, J = 6.3 Hz, 3H), 1.01 (s, 3H), 0.87 (s, 3H) ppm. MS (+ESI) m/z: 430.03 [M+H]$^+$.

4.1.34. i-Butyl 4-(biphenyl-4-yl)-2,7,7-trimethyl-5-oxo-1,4,5,6,7,8-hexahydroquinoline-3-carboxylate (53)

The title compound was obtained according to the general procedure using *i*-butyl bromide as the alkylation reagent. Yellow solid; yield: 22%. TLC: R$_f$ = 0.28 (cyclohexane/EtOAc, 2:1). ^{1}H NMR

(400 MHz, DMSO-d$_6$): δ = 9.13 (br s, 1H), 7.58 (m, 2H), 7.48 (m, 2H), 7.41 (m, 2H), 7.31 (m, 1H), 7.24 (m, 2H), 4.92 (s, 1H), 3.73 (m, 2H), 2.42 (m, 1H), 2.33 (s, 3H), 2.29 (m, 1H), 2.18 (m, 1H), 1.99 (m, 1H),1.82 (m, 1H), 1.00 (s, 3H), 0.84 (s, 3H), 0.82 (m, 9H) ppm. MS (+ESI) *m/z*: 444.04 [M+H]$^+$.

4.1.35. Cyclopentyl 4-(biphenyl-4-yl)-2,7,7-trimethyl-5-oxo-1,4,5,6,7,8-hexahydroquinoline-3-carboxylate (52)

The title compound was obtained according to the general procedure using cyclopentyl bromide as the alkylation reagent. Yellow solid; yield: 14%. TLC: R$_f$ = 0.30 (cyclohexane/EtOAc, 2:1). ^{1}H NMR (400 MHz, DMSO-d$_6$): δ = 9.04 (br s, 1H), 7.59 (m, 2H), 7.48 (m, 2H), 7.42 (m, 2H), 7.31 (m, 1H), 7.23 (m, 2H), 5.01 (m, 1H), 4.84 (s, 1H), 2.41 (m, 1H), 2.30 (m, 4H), 2.17 (m, 1H), 1.99 (m, 1H), 1.57 (m, 8H), 1.01 (s, 3H), 0.86 (s, 3H) ppm. MS (+ESI) *m/z*: 444.04 [M+H]$^+$.

4.1.36. General procedure for the Suzuki-coupling

A mixture of 1 eq of ethyl 4-(4-bromophenyl)-2,7,7-trimethyl-5-oxo-1,4,5,6,7,8-hexahydroquinoline-3-carboxylate (7), 1.5 eq of the corresponding boronic acid, 0.1 eq of tetrakis(triphenylphosphine) palladium(0), and a 2 M Na$_2$CO$_3$-solution (1.5 mL/mmol) in a 2-propanol/water-mixture (85:15) (35 mL/mmol) was subjected to a microwave vial which was then irradiated (110 °C, 120 W) for 10 min. After evaporation of the solvent under reduced pressure, the residue was taken up in EtOAc (200 mL/mmol) and washed with water (3 × 200 mL/mmol). After drying with MgSO$_4$ the solvent was removed and the crude product was purified via flash chromatography (cyclohexane/EtOAc).

4.1.37. Ethyl 4-(4-(4-trifluoromethylphenyl)phenyl)-2,7,7-trimethyl-5-oxo-1,4,5,6,7,8-hexahydroquinoline-3-carboxylate (22)

The title compound was obtained according to the general procedure using 4-trifluoromethylphenylboronic acid as the corresponding boronic acid. Colorless solid; yield: 77%. TLC: R$_f$ = 0.43 (cyclohexane/EtOAc, 1:1). ^{1}H NMR (500 MHz, DMSO-d$_6$): δ = 9.09 (br s, 1H), 7.82 (m, 2H), 7.76 (m, 2H), 7.57 (m, 2H), 7.28 (m, 2H), 4.92 (s, 1H), 4.00 (q, J = 7.3 Hz, 2H), 2.43 (m, 1H), 2.33 (m, 1H), 2.31 (s, 3H), 2.18 (m, 1H), 2.00 (m, 1H), 1.15 (t, J = 7.3, 3H), 1.02 (s, 3H), 0.88 (s, 3H) ppm. MS (+ESI) *m/z*: 484.20 [M+H]$^+$.

4.1.38. Ethyl 2,7,7-trimethyl-4-(4-(4-methylsulfonylphenyl) phenyl)-5-oxo-1,4,5,6,7,8-hexahydroquinoline-3-carboxylate (23)

The title compound was obtained according to the general procedure using 4-methylsulfonylphenylboronic acid as the corresponding boronic acid. Colorless solid; yield: 77%. TLC: R$_f$ = 0.44 (cyclohexane/EtOAc, 1:3). ^{1}H NMR (500 MHz, DMSO-d$_6$): δ = 9.1 (br s, 1H), 7.95 (m, 2H), 7.87 (m, 2H), 7.59 (m, 2H), 7.29 (m, 2H), 4.92 (s, 1H), 4.00 (q, J = 7.1 Hz, 2H), 3.23 (s, 3H), 2.44 (m, 1H), 2.32 (m, 4H), 2.18 (m, 1H), 2.00 (m, 1H), 1.15 (t, J = 7.1, 3H), 1.02 (s, 3H), 0.88 (s, 3H) ppm. MS (+ESI) *m/z*: 494.02 [M+H]$^+$.

4.1.39. Ethyl 4-(4-(4-chlorophenyl)phenyl)-2,7,7-trimethyl-5-oxo-1,4,5,6,7,8-hexahydroquinoline-3-carboxylate (24)

The title compound was obtained according to the general procedure using 4-chlorophenylboronic acid as the corresponding boronic acid. Colorless solid; yield: 76%. TLC: R$_f$ = 0.46 (cyclohexane/EtOAc, 1:1). ^{1}H NMR (500 MHz, DMSO-d$_6$): δ = 9.07 (s, 1H), 7.61 (m, 2H), 7.49 (m, 2H), 7.46 (m, 2H), 7.24 (m, 2H), 4.90 (s, 1H), 3.99 (q, J = 7.3 Hz, 2H), 2.42 (m, 1H), 2.32 (m, 1H), 2.30 (s, 3H), 2.17 (m, 1H), 1.99 (m, 1H), 1.15 (t, J = 7.3 Hz, 3H), 1.04 (s, 3H), 0.87 (s, 3H) ppm. MS (+ESI) *m/z*: 450.03 [M+H]$^+$.

4.1.40. Ethyl 4-(4-(4-fluorophenyl)phenyl)-2,7,7-trimethyl-5-oxo-1,4,5,6,7,8-hexahydroquinoline-3-carboxylate (25)

The title compound was obtained according to the general procedure using 4-fluorophenylboronic acid as the corresponding boronic acid. Colorless solid; yield: 72%. TLC: R$_f$ = 0.41 (cyclohexane/EtOAc, 1:1). ^{1}H NMR (500 MHz, DMSO-d$_6$): δ = 9.07 (s, 1H), 7.63 (m, 2H), 7.46 (m, 2H), 7.23 (m, 4H), 4.90 (s, 1H), 3.99 (q, J = 7.3 Hz, 2H), 2.43 (m, 1H), 2.31 (m, 1H), 2.30 (s, 3H), 2.17 (m, 1H), 2.00 (m, 1H), 1.15 (t, J = 7.3 Hz, 3H), 1.02 (s, 3H), 0.87 (s, 3H) ppm. MS (+ESI) *m/z*: 434.20 [M+H]$^+$.

4.1.41. Ethyl 4-(4-(4-trifluoromethoxyphenyl)phenyl)-2,7,7-trimethyl-5-oxo-1,4,5,6,7,8-hexahydroquinoline-3-carboxylate (26)

The title compound was obtained according to the general procedure using 4-trifluoromethoxyphenylboronic acid as the corresponding boronic acid. Colorless solid; yield: 52%. TLC: R$_f$ = 0.66 (cyclohexane/EtOAc, 1:1). ^{1}H NMR (500 MHz, DMSO-d$_6$): δ = 9.08 (s, 1H), 7.71 (m, 2H), 7.50 (m, 2H), 7.40 (m, 2H), 7.25 (m, 2H), 4.90 (s, 1H), 3.99 (q, J = 7.3 Hz, 2H), 2.43 (m, 1H), 2.32 (m, 4H), 2.18 (m, 1H), 2.00 (m, 1H), 1.15 (t, J = 7.3 Hz, 3H), 1.02 (s, 3H), 0.87 (s, 3H) ppm. MS (+ESI) *m/z*: 500.10 [M+H]$^+$.

4.1.42. Ethyl 4-(4-(4-cyanophenyl)phenyl)-2,7,7-trimethyl-5-oxo-1,4,5,6,7,8-hexahydroquinoline-3-carboxylate (27)

The title compound was obtained according to the general procedure using 4-cyanophenylboronic acid as the corresponding boronic acid. Colorless solid; yield: 50%. TLC: R$_f$ = 0.36 (cyclohexane/EtOAc, 1:1). ^{1}H NMR (500 MHz, DMSO-d$_6$): δ = 9.10 (br s, 1H), 7.87 (m, 2H), 7.81 (m, 2H), 7.58 (m, 2H), 7.28 (m, 2H), 4.91 (s, 1H), 3.98 (q, J = 7.3 Hz, 2H), 2.43 (m, 1H), 2.31 (m, 1H), 2.30 (s, 3H), 2.17 (m, 1H), 2.00 (m, 1H), 1.14 (t, J = 7.3 Hz, 3H), 1.01 (s, 3H), 0.86 (s, 3H) ppm. MS (+ESI) *m/z*: 441.06 [M+H]$^+$.

4.1.43. Ethyl 4-(4-(4-pyridyl)phenyl)-2,7,7-trimethyl-5-oxo-1,4,5,6,7,8-hexahydroquinoline-3-carboxylate (28)

The title compound was obtained according to the general procedure using 4-pyridylboronic acid as the corresponding boronic acid. Colorless solid; yield: 46%. TLC: R$_f$ = 0.38 (cyclohexane/EtOAc, 1:3). ^{1}H NMR (500 MHz, DMSO-d$_6$): δ = 9.10 (s, 1H), 8.58 (m, 2H), 7.63 (m, 2H), 7.55 (m, 2H), 7.29 (m, 2H), 4.92 (s, 1H), 3.99 (q, J = 7.3 Hz, 2H), 2.43 (m, 1H), 2.32 (m, 1H), 2.31 (s, 3H), 2.19 (m, 1H), 2.00 (m, 1H), 1.14 (t, J = 7.3 Hz, 3H), 1.01 (s, 3H), 0.86 (s, 3H) ppm. MS (+ESI) *m/z*: 417.36 [M+H]$^+$.

4.1.44. Ethyl 2,7,7-trimethyl-4-(4-(4-methylphenyl)phenyl)-5-oxo-1,4,5,6,7,8-hexahydroquinoline-3-carboxylate (29)

The title compound was obtained according to the general procedure using 4-methylphenylboronic acid as the corresponding boronic acid. Colorless solid; yield: 39%. TLC: R$_f$ = 0.45 (cyclohexane/EtOAc, 1:1). ^{1}H NMR (500 MHz, DMSO-d$_6$): δ = 9.06 (s, 1H), 7.48 (m, 2H), 7.45 (m, 2H), 7.22 (m, 2H), 7.21 (m, 2H), 4.89 (s, 1H), 4.00 (q, J = 7.3 Hz, 2H), 2.42 (m, 1H), 2.32 (s, 3H), 2.31 (m, 1H), 2.30 (s, 3H), 2.17 (m, 1H), 2.00 (m, 1H), 1.15 (t, J = 7.3 Hz, 3H), 1.02 (s, 3H), 0.88 (s, 3H) ppm. MS (+ESI) *m/z*: 430.01 [M+H]$^+$.

4.1.45. Ethyl 2,7,7-trimethyl-4-(4-(4-N,N-dimethylaminophenyl) phenyl)-5-oxo-1,4,5,6,7,8-hexahydroquinoline-3-carboxylate (30)

The title compound was obtained according to the general procedure using 4-N,N-dimethylaminophenylboronic acid as the corresponding boronic acid. Colorless solid; yield: 36%. TLC: R$_f$ = 0.35 (cyclohexane/EtOAc, 1:1). ^{1}H NMR (500 MHz, DMSO-d$_6$): δ = 9.03 (s, 1H), 7.44 (m, 2H), 7.37 (m, 2H), 7.16 (m, 2H), 6.76 (m, 2H), 4.86 (s, 1H), 3.98 (q, J = 7.3 Hz, 2H), 2.91 (s, 6H), 2.42 (m, 1H), 2.30 (m, 4H), 2.17 (m, 1H), 1.99 (m, 1H), 1.16 (t, J = 7.3 Hz, 3H), 1.02 (s, 3H), 0.88 (s, 3H) ppm. MS (+ESI) *m/z*: 459.21 [M+H]$^+$.

4.1.46. Ethyl 4-(4-(4-methoxyphenyl)phenyl)-2,7,7-trimethyl-5-oxo-1,4,5,6,7,8-hexahydroquinoline-3-carboxylate (31)

The title compound was obtained according to the general procedure using 4-methoxyphenylboronic acid as the corresponding boronic acid. Colorless solid; yield: 25%. TLC: $R_f = 0.11$ (cyclohexane/EtOAc, 2:1). ^{1}H NMR (400 MHz, DMSO-d$_6$): $\delta = 9.09$ (br s, 1H), 7.53 (m, 2H), 7.43 (m, 2H), 7.20 (m, 2H), 6.97 (m, 2H), 4.88 (s, 1H), 3.99 (q, $J = 7.0$ Hz, 2H), 3.77 (s, 3H), 2.43 (m, 1H), 2.33 (m, 1H), 2.29 (s, 3H), 2.18 (m, 1H), 1.99 (m, 1H), 1.15 (t, $J = 7.0$ Hz, 3H), 1.01 (s, 3H), 0.87 (s, 3H) ppm. MS (+ESI) m/z: 445.91 [M+H]$^+$.

4.1.47. Ethyl 4-(4-(4-hydroxyphenyl)phenyl)-2,7,7-trimethyl-5-oxo-1,4,5,6,7,8-hexahydroquinoline-3-carboxylate (32)

The title compound was obtained according to the general procedure using 4-t-butyldimethylsilyloxyphenylboronic acid as the corresponding boronic acid. After purification the protecting group was cleaved. For this, the 1 eq of the intermediate was dissolved in THF (30 mL/mmol) and a drop of methanol. This mixture was cooled to 0 °C and 1.5 eq. of a 1 M tetrabutylammonium fluoride (TBAF) solution in THF was added. After 1.5 h at 0 °C the reaction was quenched by the addition of EtOAc (60 mL/mmol). The organic layer was washed with a 5% NaHCO$_3$-solution and brine. After drying with MgSO$_4$, the solvent was removed under reduced pressure and the crude product was purified via flash chromatography (cyclohexane/EtOAc). Colorless solid; yield: 15% (2 steps). TLC: $R_f = 0.07$ (cyclohexane/EtOAc, 2:1). ^{1}H NMR (400 MHz, DMSO-d$_6$): $\delta = 9.49$ (s, 1H), 9.09 (br s, 1H), 7.39 (m, 4H), 7.17 (m, 2H), 6.80 (m, 2H), 4.86 (s, 1H), 3.98 (q, $J = 7.0$ Hz, 2H), 2.43 (m, 1H), 2.31 (m, 1H), 2.29 (s, 3H), 2.17 (d, 1H), 1.99 (m, 1H), 1.15 (t, $J = 7.0$ Hz, 3H), 1.01 (s, 3H), 0.87 (s, 3H) ppm. MS (+ESI) m/z: 431.97 [M+H]$^+$.

4.1.48. General synthetic procedure for the preparation of 2-amino-1,4-dihydropyidines 40, 41

In a round bottom flask 1 eq. of dimedone, 1 eq of the desired aldehyde and 1 eq of ethyl 3-amino-3-iminopropionate hydrochloride were suspended in dry EtOH (2.5 mL/mmol) and heated at 80 °C. To this solution 1 eq of a 0.5 M sodium ethanolate solution was added over the period of 20 min. After heating for further 30 min under reflux the reaction was cooled to 0 °C and water (40 mL/mmol) was added. The aqueous solution was extracted with EtOAc (5 × 20 mL/mmol). The combined organic layers were washed with brine, dried with MgSO$_4$ and the solvent was evaporated under reduced pressure. The crude material was purified by recrystallization from ethanol.

4.1.49. Ethyl 4-(biphenyl-4-yl)-2-amino-7,7-dimethyl-5-oxo-1,4,5,6,7,8-hexahydroquinoline-3-carboxylate (40)

The title compound was obtained according to the general procedure using 4-biphenylcarboxaldehyde as the corresponding aldehyde component. Yellow solid; yield: 12%. TLC: $R_f = 0.16$ (cyclohexane/EtOAc, 1:1). ^{1}H NMR (500 MHz, DMSO-d$_6$): $\delta = 8.88$ (br s, 1H), 7.59 (m, 2H), 7.46 (m, 2H), 7.41 (m, 2H), 7.30 (m, 1H), 7.23 (m, 2H), 6.77 (br s, 2H), 4.77 (s, 1H), 3.94 (q, $J = 6.9$ Hz, 2H), 2.43 (m, 1H), 2.31 (m, 1H), 2.18 (m, 1H), 1.99 (m, 1H), 1.13 (t, $J = 6.9$ Hz, 3H), 1.03 (s, 3H), 0.89 (s, 3H) ppm. MS (+ESI) m/z: 417.14 [M+H]$^+$.

4.1.50. Ethyl 4-(4-t-butylphenyl)-2-amino-7,7-dimethyl-5-oxo-1,4,5,6,7,8-hexahydroquinoline-3-carboxylate (41)

The title compound was obtained according to the general procedure using 4-t-butylphenylcarboxaldehyde as the corresponding aldehyde component. Yellow solid; yield: 20%. TLC: $R_f = 0.59$ (cyclohexane/EtOAc, 1:1). ^{1}H NMR (500 MHz, DMSO-d$_6$): $\delta = 8.83$ (br s, 1H), 7.16 (m, 2H), 7.05 (m, 2H), 6.70 (br s, 2H), 4.70 (s, 1H), 3.94 (q, $J = 7.4$ Hz, 2H), 2.40 (m, 1H), 2.31 (m, 1H), 2.15 (m, 1H), 1.98 (m, 1H), 1.21 (s, 9H), 1.13 (t, $J = 7.4$ Hz, 3H), 1.02 (s, 3H) 0.90 (s,

3H) ppm. MS (+ESI) m/z: 397.19 [M+H]$^+$.

4.1.51. Diastereomeric resolution for the preparation of the single enantiomers of ethyl 4-(biphenyl-4-yl)-2,7,7-trimethyl-5-oxo-1,4,5,6,7,8-hexahydroquinoline-3-carboxylate [8]

1 eq of (2S,3R)-methyl 2-(3-nitrobenzamido)-3-(3-oxobutanoyloxy)butanoate [8], 1 eq of 4-biphenylcarboxaldehyde, 1 eq. of dimedone, 1 eq of dried NH$_4$OAc, and 0.3 eq of iodine were stirred overnight in EtOH (0.5 mL/mmol) at room temperature. Then of EtOAc (20 mL/mmol) was added to the brown slurry and washed with aqueous saturated Na$_2$S$_2$O$_3$ (2×) and brine (1×). The organic layer was dried (MgSO$_4$) and concentrated in a vacuum to afford a yellow solid foam. The crude mixture was purified by flash chromatography using a short column (cyclohexane/EtOAc). The separation of the diastereomers was performed with a preparative HPLC (isocratic elution: water, acetonitrile and methanol (30/27/43, A/B/C), flow rate: 20 mL/min over 45 min).

4.1.52. (2R,3S)-4-Methoxy-3-(3-nitrobenzamido)-4-oxobutan-2-yl 4-(biphenyl-4-yl)-2,7,7-trimethyl-5-oxo-1,4,5,6,7,8-hexahydroquinoline-3-carboxylate diastereomers (56a, b)

Diastereomer 56a: Yellow solid; 13% Analytical data are in accordance with the literature [8]; Diastereomer 56b: Yellow solid; 26% Analytical data are in accordance with the literature [8].

4.1.53. 10-(Biphenyl-4-yl)-1,9-dioxo-1,2,3,4,5,6,7,8,9,10-decahydroacridine (34)

1 eq of biphenylaldehyde and 3 eq of dimedone were dissolved in a mixture of ethanol (4 mL/mmol) and water (3 mL/mmol). After the addition of 0.1 mL/mmol piperidine, the reaction mixture was refluxed for 10 min. After cooling to room temperature, the white precipitate was filtered of, washed with water and 50% aq. ethanol yielding 72% of biphenyl-4-yl-bisdimedonylmethane. This solid was mixed with 27 eq of ammonium acetate in acetic acid (7 mL/mmol) and was refluxed for 1 h, cooled to room temperature and then diluted with water (40 mL/mmol). The precipitate was filtered off, washed with water and recrystallized from ethanol to give a light yellow powder. Yield: 58%. TLC: $R_f = 0.5$ (EtOAc/DCM, 1:2). ^{1}H NMR (400 MHz, DMSO-d$_6$): $\delta = 9.31$ (br s, 1H), 7.41 (m, 9H), 4.85 (s, 1H), 2.46 (m, 2H), 2.35 (m, 2H), 2.18 (m, 2H), 1.99 (m, 2H), 1.01 (s, 6H), 0.89 (s, 6H). MS (+ESI) m/z: 426 ([M+H]$^+$.

4.1.54. 11-(Biphenyl-4-yl)-3,3-dimethyl-1,2,3,4,5,11-hexahydroindeno[1,2-b]quinoline-1,10-dione (36)

1 eq of indan-1,3-dione and 1 eq of biphenylaldehyde were dissolved in hot acetic acid (2 mL/mmol), 2 drops of conc. sulphuric acid was added and the mixture was refluxed for 2 min. After cooling to room temperature, the light brown precipitate was filtered, washed with acetic acid, water and ethanol giving 2-(biphenyl-4-yl-methyliden)-indan-1,3-dione in 50% yield. This solid was mixed with 1.04 eq of 3-amino-5,5-dimethyl-2-cyclohexen-1-one in acetic acid (10 mL/mmol) and was refluxed for 3 min. After cooling to room temperature, a red precipitate was filtered off, washed with acetic acid, water and ethanol and recrystallized from ethanol to give red crystals. Yield: 67%. ^{1}H NMR (400 MHz, DMSO-d$_6$): $\delta = 10.44$ (br s, 1H), 7.57 (m, 3H), 7.49 (m, 2H), 7.43 (m, 3H), 7.32 (m, 4H), 7.25 (m, 1H), 4.77 (s, 1H), 2.63 (s, 2H), 2.26 (m, 1H), 2.12 (m, 1H), 1.07 (s, 3H), 1.02 (s, 3H). MS (+ESI) m/z: 432 [M+H]$^+$.

4.2. X-ray crystallography

The X-ray intensity data were measured on a Bruker D8 VENTURE system equipped with a multilayer monochromator and a Cu Kα Incoatec microfocus sealed tube ($\lambda = 1.54178$ Å). The absolute

configuration could be determined via the anormal dispersion due to a reliable flack parameter (-0.075). Experimental details regarding crystal structure, data collection and structure refinement is archived at CCDC (deposition number 1043330) and also listed in Supporting information (Tables S1–S7).

4.3. TGFβ/Smad assay

An SMAD-4 binding element (SBE-4)-based transient luciferase reporter gene assay was done in HEK293T cells as described in detail before [8]. Briefly, cells were co-transfected with an SBE-4-firefly luciferase and TK-driven renilla luciferase plasmid, replated after 12–14 h on 96-well plates and incubated for 2 h before addition of test compounds, DMSO and TGFβ-2 or Activin A (10 ng/mL). Each condition was done in triplicate. After 20–22 h, firefly and renilla luciferase activities were measured on a Tecan Infinite M1000 (Crailsheim, Germany) following the instructions of the Dual Luciferase Assay Kit (Promega, Madison, USA). Presented data was derived from typically 2–4 independent experiments unless otherwise stated. GraphPad Prism 5 was used for data evaluation.

4.4. Computational studies

4.4.1. Molecular electrostatic potential (MEP) calculations

All quantum chemical calculations were performed with the Gaussian 03 program package (revision E.01) [20] at the B3LYP/6-31 + G(d) level of theory. To elucidate the nature of a calculated stationary point harmonic vibrational frequency analyses were performed. Minima did not exhibit any imaginary frequencies. Starting structures were obtained from correlated crystal structures. Connolly surfaces (probe radius 1.0) mapped with the electrostatic potential were obtained with the Molekel program package (revision 4.2) based on the results of the corresponding quantum chemical calculations.

4.4.2. 3D-QSAR

Dataset preparation. The overall dataset for the 3D QSAR analysis contained 81 DHPs with measured activity from this study and our previous report [8] (see Supporting information for a complete overview of structures and activities of all compounds, Tables S8 and S9). The 3D conformations of all ligands were prepared in MOE (version 2013.0801) (Molecular Operating Environment (MOE), Montreal, Canada) based on the crystal structure of the active (*R*)-configured ITD-1 (+)-enantiomer (**54b**) reported here. The final alignment of the modified groups was also calculated in MOE while keeping the underlying DHP scaffold fixed. Initially, the overall dataset was randomly separated into a training dataset (58 molecules) and a test dataset (23 molecules) with focus on a homogeneous distribution of activity data. Unfortunately, the created test dataset originally contained five structural singletons (**33***, **23**, **8**, **55**) that are not represented in the training dataset. Preliminary tests showed that a test dataset containing these molecules led to a poor correlation and an apparently non-predictive model. They were not well-predicted due to the lack of similar analogs in the training data set (4″-sulfone **23**, tricyclic lactam **55**, 4′-indole **33***, 4′-ethinyl **8**). Therefore, these compounds are outside the chemical space that was used to train the model, and thus, could not be predicted correctly and were removed from the test dataset. The final test dataset thus contained 19 molecules.

3D-QSAR analysis. The 3D-QSAR analysis was performed using the freely-available open-source software Open3DQSAR (http://open3dqsar.sourceforge.net/) [21]. The molecular interactions fields (MIFS) in Open3DQSAR are calculated according to a Lennard-Jones' 6–12 potential and an sp3 carbon atom probe representing Van-der-Waals interactions (the steric field) and by summing up coulomb interactions of a positively charged probe (the electrostatic field). The calculations were performed in a grid of 29 Å × 28 Å × 26 Å with, an edge length of 1 Å. Both MIFs were scaled after applying a cut-off of ±30.0 kcal/mol and variables with a standard deviation < 0.1 were removed. The smart region definition algorithm implemented in Open3DQSAR was used to remove less important variables and group spatially adjacent fields. Using the partial least square (PLS) method the molecular interaction fields were correlated with the biological data.

Validation. The leave-one-out (LOO) and leave-many-out (LMO) methods were used for internal cross-validation. For LMO validation the dataset was 20 times randomly grouped into five groups, whereas the activity of one of these groups is than predicted based on a QSAR model of the remaining four groups. For LOO validation, only one molecule is neglected and predicted by the remaining molecules. Finally, the test dataset was used to evaluate the quality of the create QSAR model, by predicting the biological activity.

Visualization. The coefficients of the molecular interaction fields from the 3D-QSAR model were visualized using MOE (Molecular Operating Environment (MOE), Montreal, Canada). The used contour levels for the different surfaces were: Electrostatic positive (blue): 0.015, electrostatic negative (red): −0.015, vdw positive (green): 0.025 and vdw negative (yellow): −0.01.

Acknowledgment

Appendix A. Supplementary data

Supplementary data related to this article can be found at http://dx.doi.org/10.1016/j.ejmech.2015.03.027.

References

[1] R. Derynck, K. Miyazono, TGFβ and the TGFβ family, in: R. Derynck, K. Miyazono (Eds.), The TGFβ Family, Cold Spring Harbor Laboratory Press, Cold Spring Harbor, New York, 2008, pp. 29–43.
[2] K. Wharton, R. Derynck, TGFbeta family signaling: novel insights in development and disease, Development 136 (2009) 3691–3697.
[3] J.M. Yingling, K.L. Blanchard, J.S. Sawyer, Development of TGF-beta signalling inhibitors for cancer therapy, Nat. Rev. Drug Discov. 3 (2004) 1011–1022.
[4] N.S. Nagaraj, P.K. Datta, Targeting the transforming growth factor-beta signaling pathway in human cancer, Expert Opin. Investig. Drugs 19 (2010) 77–91.
[5] D. Bonafoux, W.C. Lee, Strategies for TGF-beta modulation: a review of recent patents, Expert Opin. Ther. Pat. 19 (2009) 1759–1769.
[6] D. Langle, J. Halver, B. Rathmer, E. Willems, D. Schade, Small molecules targeting in vivo tissue regeneration, ACS Chem. Biol. 9 (2014) 57–71.
[7] E. Willems, J. Cabral-Teixeira, D. Schade, W. Cai, P. Reeves, P.J. Bushway, M. Lanier, C. Walsh, T. Kirchhausen, J.C. Izpisua Belmonte, J. Cashman, M. Mercola, Small molecule-mediated TGF-beta type II receptor degradation promotes cardiomyogenesis in embryonic stem cells, Cell Stem Cell 11 (2012) 242–252.
[8] D. Schade, M. Lanier, E. Willems, K. Okolotowicz, P. Bushway, C. Wahlquist, C. Gilley, M. Mercola, J.R. Cashman, Synthesis and SAR of b-annulated 1,4-dihydropyridines define cardiomyogenic compounds as novel inhibitors of TGFbeta signaling, J. Med. Chem. 55 (2012) 9946–9957.
[9] H. Meyer, F. Bossert, H. Horstmann, Liebigs Ann. Chem. (1977) 1895–1908.
[10] M. Petrova, R. Muhamadejev, B. Vigante, B. Cekavicus, A. Plotniece, G. Duburs, E. Liepinsh, Intramolecular C-H···O hydrogen bonding in 1,4-dihydropyridine derivatives, Molecules 16 (2011) 8041–8052.
[11] S.A. Steiger, A.J. Monacelli, C. Li, J.L. Hunting, N.R. Natale, Diethyl 4-(biphenyl-4-yl)-2,6-dimethyl-1,4-di-hydro-pyridine-3,5-di-carboxyl-ate, Acta Crystallogr. Sect. E Struct. Rep. Online 70 (2014) o791–792.
[12] M.M. Kurbanova, E.Z. Huseynov, A.V. Gurbanov, A.M. Maharramov, S.W. Ng,

Ethyl 2,7,7-trimethyl-5-oxo-4-phenyl-1,4,5,6,7,8-hexa-hydro-quinoline-3-carboxyl-ate, Acta Crystallogr. Sect. E Struct. Rep. Online 68 (2012) o2233.

[13] J. Verma, V.M. Khedkar, E.C. Coutinho, 3D-QSAR in drug design – a review, Curr. Top. Med. Chem. 10 (2010) 95–115.

[14] C. Hansch, T. Fujito, p-σ-π analysis. A method for the correlation of biological activity and chemical structure, J. Am. Chem. Soc. 86 (1964) 1616–1626.

[15] S.M. Free Jr., J.W. Wilson, A mathematical contribution to structure-activity studies, J. Med. Chem. 7 (1964) 395–399.

[16] A. Radadiya, V. Khedkar, A. Bavishi, H. Vala, S. Thakrar, D. Bhavsar, A. Shah, E. Coutinho, Synthesis and 3D-QSAR study of 1,4-dihydropyridine derivatives as MDR cancer reverters, Eur. J. Med. Chem. 74 (2014) 375–387.

[17] V.S. Mathura, N. Patel, C. Bachmeier, M. Mullan, D. Paris, A 3D-QSAR model based screen for dihydropyridine-like compound library to identify inhibitors of amyloid beta (Abeta) production, Bioinformation 5 (2010) 122–127.

[18] P.S. Kharkar, B. Desai, H. Gaveria, B. Varu, R. Loriya, Y. Naliapara, A. Shah, V.M. Kulkarni, Three-dimensional quantitative structure-activity relationship of 1,4-dihydropyridines as antitubercular agents, J. Med. Chem. 45 (2002) 4858–4867.

[19] R. Miri, K. Javidnia, B. Hemmateenejad, M. Tabarzad, M. Jafarpour, Synthesis, evaluation of pharmacological activities and quantitative structure-activity relationship studies of a novel group of bis(4-nitroaryl-1,4-dihyropyridine), Chem. Biol. Drug Des. 73 (2009) 225–235.

[20] M.J. Frisch, G.W. Trucks, H.B. Schlegel, G.E. Scuseria, M.A. Robb, J.R. Cheeseman, J.A. Montgomery Jr., T. Vreven, K.N. Kudin, J.C. Burant, J.M. Millam, S.S. Iyengar, J. Tomasi, V. Barone, B. Mennucci, M. Cossi, G. Scalmani, N. Rega, G.A. Petersson, H. Nakatsuji, M. Hada, M. Ehara, K. Toyota, R. Fukuda, J. Hasegawa, M. Ishida, T. Nakajima, Y. Honda, O. Kitao, H. Nakai, M. Klene, X. Li, J.E. Knox, H.P. Hratchian, J.B. Cross, V. Bakken, C. Adamo, J. Jaramillo, R. Gomperts, R.E. Stratmann, O. Yazyev, A.J. Austin, R. Cammi, C. Pomelli, J.W. Ochterski, P.Y. Ayala, K. Morokuma, G.A. Voth, P. Salvador, J.J. Dannenberg, V.G. Zakrzewski, S. Daniels, A.D. Daniels, M.C. Strain, O. Farkas, D.K. Malick, A.D. Rabuck, K. Raghavachari, J.B. Foresman, J.V. Ortiz, Q. Cui, A.G. Baboul, S. Clifford, J. Cioslowski, B.B. Stefanov, G. Liu, A. Liashenko, P. Piskorz, I. Komaromi, R.L. Martin, D.J. Fox, T. Keith, M.A. Al-Laham, C.Y. Peng, A. Nanayakkara, M. Challacombe, P.M.W. Gill, B. Johnson, W. Chen, M.W. Wong, C. Gonzalez, J.A. Pople, Gaussian 03, Revision E.01, Gaussian, Inc., Wallingford CT, 2004.

[21] P. Tosco, T. Balle, Open3DQSAR: a new open-source software aimed at high-throughput chemometric analysis of molecular interaction fields, J. Mol. Model. 17 (2011) 201–208.